COPPER INSERTION IN A SERIES OF METAL-ORGANIC FRAMEWORKS WITH UNCOORDINATED CARBOXYLIC ACID GROUPS FOR AMMONIA REMOVAL

A Thesis
Presented to
The Academic Faculty

By

Erika Y. Garcia-Gutierrez

In Partial Fulfillment
Of the Requirements for the Degree
Master of Science in the
School of Chemical and Biomolecular Engineering

Georgia Institute of Technology
August 2015

COPPER INSERTION IN A SERIES OF METAL ORGANIC FRAMEWORKS

WITH UNCOORDINATED CARBOXYLIC ACID GROUPS

FOR AMMONIA REMOVAL

Approved by:

Dr. Krista S. Walton, Advisor
School of Chemical and Biomolecular Engineering
Georgia Institute of Technology

Dr. Ryan P. Lively
School of Chemical and Biomolecular Engineering
Georgia Institute of Technology

Dr. Carson Meredith
School of Chemical and Biomolecular Engineering
Georgia Institute of Technology

Date Approved: June 12, 2015.

To my dad, Eric Garcia

ACKNOWLEDGEMENTS

I would like to give special thanks to my advisor, Dr. Krista Walton for her guidance and support, but more specifically, for her understanding when I decided to change to the Master's program. It was her understanding and comfort, that gave me the strength and determination to make one of the most important decisions in my career, and for that, I will be forever grateful.

It has been a great honor to be part of the Walton Research Group. Each and every one of the group members have helped me at some point in these (almost) two years, either by training me in different equipment or by providing counsel and guidance throughout my research project. For that and so many other reasons, I would like to deeply appreciate all the former and current group members (Dr. Grabicka, Dr. Stults, Dr. Jasuja, Dr. Cmarik, Dr. Duerinck, Dr. Morelock, Dr. Murdock, Karen, Mike, Jacob, Colton, Julian, Michael, William, Lalit, Nick, and Yang) for their help and support during this whole process.

It is from the bottom of my heart, that I give special thanks to Karen Tulig. There were many, many times in which she helped shape and focus my work. Every time I felt frustrated, confused and lost, she was there to discuss every detail of my experiments with me and give me advice.

I would also like to thank my committee members, Dr. Carson Meredith and Dr. Ryan P. Lively, for all their help and insight; Dr. Bogna Grabicka, for always caring and helping me since my first day in the lab; Dr. Chris Murdock, for always taking the time to talk and discuss the experiments with me; Michael Dutzer, for helping with the

unfortunate waste container incident; and to Michael Mangarella for training me on the breakthrough system and for collecting the XPS data for this work. Additionally, I would like to thank Dr. David Tavakoli for his tremendous help with the XRD, I will be forever thankful.

Last but not least, I am profoundly thankful for my friends, specially, Legna, Ricardo and Kassandra; and my family, which is my biggest blessing. This is as yours, as it is mine.

TABLE OF CONTENTS

LIST OF TABLES

LIST OF FIGURES

LIST OF SYMBOLS AND ABBREVIATIONS

P	Pressure
P_O	Saturation Vapor Pressure
NH_3	Ammonia
$Cu(BF_4)_2$	Copper tetrafluoroborate
$Cu(NO_3)_2$	Copper nitrate
eV	Electron Volt
^oC	Degree Celsius
Å	Angstrom
K	Kelvin
RH	Relative Humidity
ppm	Parts per Million
mg	Milligram
mL	Milliliters
m^2	Meter Squared
cm^3	Cubic Centimeter
mmol	Millimole
min	Minute
MOF	Metal–Organic Frameworks
PCP	Porous Coordination Polymers
PSM	Post Synthetic Modification
CWA	Chemical Warfare Agents

TIC	Toxic Industrial Chemicals
CBRN	Chemical, Biological, Radiological And Nuclear
BTC	1,3,5-Benzenetricarboxylic Acid
BDC	1,2,4-Benzenedicarboxylic Acid
BDC-COOH	1,2,4-Benzenetricarboxylic Acid
BDC-$(COOH)_2$	1,2,4,5-Benzenetetracarboxylic Acid
DMF	N,N-Dimethylformamide
DMA	N,N-Dimethyacetamide
PXRD	Powder X-Ray Diffraction
BET	Brunauer, Emmett, And Teller
ICP-OES	Inductively Coupled Plasma Optical Emission Spectrometry
XPS	X-Ray Photoelectron Spectroscopy
TGA	Thermo-Gravimetric Analysis
EPR	Electron Paramagnetic Resonance
EXAFS	Extended X-Ray Adsorption Fine Structure
DFT	Density Functional Theory
RT	Room Temperature

SUMMARY

Metal-organic frameworks are a widely studied class of porous crystalline materials characterized by their high surface areas, porosity and thermal stability. Recent research studies have identified these materials as potential candidates for a wide variety of applications including catalysis, gas adsorption and drug delivery. Among these applications, air purification is of great importance given the need to improve current filter materials to include protection against gases with high vapor pressures such as ammonia. In order to achieve this, materials must be water-stable and, at the same time, have strong interaction sites with ammonia.

To this end, this thesis presents the first step in analyzing the performance of MOFs with copper carboxylate functional groups toward ammonia removal from air. The insertion of copper atoms into the UiO-66-COOH and UiO-66-$(COOH)_2$ frameworks was attained by a post-synthetic modification of the materials. Results gathered in this study show that metal loading is highly limited by the pore space available for metal complexation.

Ammonia breakthrough experiments presented here demonstrate that the metalated materials perform better than UiO-66-COOH and UiO-66-$(COOH)_2$ under dry and humid conditions. In particular, to the best of our knowledge, UiO-66-$(COOCu)_2$ has the highest ammonia dynamic capacity among other UiO-66 functionalities. Recommendations for future work are focused on a more extensive characterization of the copper coordination environment after metalation and subsequent methods for increasing metal loading on the materials.

CHAPTER 1

INTRODUCTION

Metal–organic frameworks (MOFs), also known as porous coordination polymers (PCPs), are an emerging class of porous crystalline materials consisting of metal clusters linked together by organic ligands.[1-3] Since their discovery, MOFs have attracted considerable attention due to their high surface areas and porosity,[4,5] which make them attractive candidates for gas adsorption applications such as gas storage[6,7] and separation,[8,9] catalysis,[10] air purification,[11-12] drug delivery,[13] gas sensing,[14] among others. With more than thousands of metal-organic structures already registered in the Cambridge Structure Database, these hybrid materials represent an alternative over other current and common sorbent materials, such as zeolites and activated carbons.[2] One advantage of MOFs over other porous materials is that their chemical properties can be easily tailored by incorporating different reactive functional groups, either by selecting specific inorganic and organic building blocks, or by post synthetic modification (PSM) of the frameworks.[15,16] It is this high tailorability, in addition to their high thermal stability (usually higher than 500 K) and high porosities, which make them ideal candidates to be used as filter materials in air purification of toxic chemicals applications.[12,17]

The effective filtration of toxic chemicals, including chemical warfare agents (CWAs) and toxic industrial chemicals (TICs), is of great importance given the risks associated with exposure to these harmful gases. Current filtration media used in chemical, biological, radiological and nuclear (CBRN) breathing protection devices

consist of carbon impregnated with copper, silver, zinc, molybdenum, and triethylenediamine (TEDA).[18] This material, known as ASZM-TEDA, does not provide enough or adequate protection against chemicals with high vapor pressures (i.e. greater than 100 mm Hg), such as carbon monoxide, carbon dioxide, nitric oxide, nitrogen dioxide, ammonia and metal carbonyls.[19] In particular, ammonia (NH_3) is a highly toxic gas with a vapor pressure of 7600 mm Hg at 25°C,[20] and one of the most commonly produced industrial chemicals in the United States.[21] Ammonia production is estimated in more than 10 million metric tons per year in the United States alone with its most significant use in the agricultural application of fertilizers, which accounts for more than 80% of the commercially produced ammonia.[22] With other applications in refrigeration, as a component of household cleaners and in the production of explosives, plastics, synthetic fibers and resins, ammonia has been identified as one of the chemicals with high risk for spill accidents.[12,23] The copious ammonia production facilities worldwide and its numerous uses also imply that exposure may be caused not only by accidental spills but also by terrorist attacks.[21] Previous uses of ammonia as a toxic weapon include the attack by Serbian forces (in the 1990s) to chemical facilities that stored anhydrous ammonia in large amounts.[24]

For this and many other reasons, it is imperative to design better filter materials for breathing protection devices for soldiers and first responders who may be exposed to TICs such as ammonia. In recent years, MOFs have been evaluated as potential candidates to be used in CBRN filters due to their high porosity and their ability to have reactive functional groups covalently coordinated to the frameworks.[25-30] Previous research studies have found that MOFs with coordinatively unsaturated metal centers,

such as Cu-BTC (HKUST-1) and MOF-74, exhibit high ammonia capacities due to the ability of ammonia to covalently bind to the open metal sites. Unfortunately, both materials exhibit a loss in capacity and porosity under humid conditions. Peterson et al.[32] examined the ammonia capacity of Cu-BTC under dry and humid conditions at 293 K, and found a higher uptake under humid (80% RH) conditions (8.9 mmol g^{-1}) than under dry (0% RH) conditions (6.6 mmol g^{-1}). It is hypothesized that this increase in the ammonia capacity is caused by the formation of ammonium salts of the BTC (BTC= 1,3,5-benzenetricarboxylic acid) linker. Upon a second exposure to ammonia, both samples showed a loss in capacity of 57% and 89% under dry and humid conditions, respectively. The apparent surface area of the materials was also significantly reduced after ammonia exposure, which indicates a loss in porosity and a permanent change in the Cu-BTC structure. Yaghi and coworkers[33] studied the performance of several (Co, Mg, Ni, Zn) MOF-74 analogues in toxic gas adsorption and found that all the materials outperformed the ammonia capacities of both BPL carbon and 13X zeolite under dry conditions (except for Ni-MOF-74), which was attributed to adsorbent-adsorbate interactions between ammonia and the open metal sites. Under humid conditions (RH=80%), the dynamic loadings of ammonia on all the MOF-74 analogues were significantly reduced, possibly due to the competitive adsorption of water.

Although these and several other studies have advanced our understanding of ammonia adsorption on MOFs, it is necessary to expand these studies to water stable materials. Motivated by this fact, Jasuja et al.[26] investigated the performance of several functionalized ($-NH_2$, $-NO_2$, -OH, $-(OH)_2$, $-SO_3H$, $-(COOH)_2$) versions of UiO-66 (or Zr-BDC), a MOF that possesses exceptional stability under humid conditions.[34-37] From all

of the Zr-MOFs included in the study, UiO-66-OH and UiO-66-NH_2 showed the highest capacities for ammonia under both dry and humid conditions. Under humid conditions, the ammonia loading at saturation was 2.77 mmol g^{-1} and 3.01 mmol g^{-1} for UiO-66-OH and UiO-66-NH_2, respectively. Reduced pore space within the materials, caused by the introduction of bulky functional groups, was found to limit the ammonia capacities of the materials with acidic functional groups such as $–(COOH)_2$ and $–SO_3H$.

Computational methods have also been employed as a screening method to identify functional groups that react or bind strongly with ammonia.[25,38] Snurr and coworkers[25] used quantum chemical methods to calculate the binding energies of both ammonia and water, with several functional groups grafted into a naphthalene molecule (representative aromatic backbone). From the 21 different functional groups studied, R-COOCu and R-COOAg (R= naphthalene molecule) had the highest binding energies of ammonia (-161.2 kJ mol^{-1} and -84.9 kJ mol^{-1} for R-COOCu and R-COOAg, respectively) and the strongest preference for ammonia over water. Electron-deficient metal atoms, such as Cu and Ag, are expected to interact strongly with the ammonia nitrogen atom. While this and other studies help identify functional groups that react strongly with ammonia, there are synthetic challenges that need to be overcome in order to experimentally test these materials for ammonia capture. In most part, these synthesis issues come from possible interactions between the desired functional groups and the metal nodes. To avoid these and other synthetic issues caused by using prefunctionalized linkers, several studies have been made on the post synthetic modification of carboxylate groups to generate metal carboxylates. As an example, Gadzikwa et al.[39] successfully incorporated COO-Cu-OOC into a Zn-based, mixed-ligand MOF. Similarly, Meng et al.[40]

incorporated Cu^{2+}, Ni^{2+}, Co^{2+} and Cd^{2+} ions into a Zn-based MOF decorated with uncoordinated carboxyl groups.

In this thesis, we develop a post synthetic modification technique to create copper carboxylate groups into the water stable MOF UiO-66. The objectives of this study were two-fold:

1. Create copper carboxylate functional groups by a post synthetic modification of the UiO-66-COOH and UiO-66-$(COOH)_2$ frameworks and identify the different parameters that affect the metal insertion. Figure 1 shows a schematic representation of the copper insertion into the UiO-66-COOH framework.

2. Investigate the ammonia adsorption capacities of these materials under dry and humid conditions.

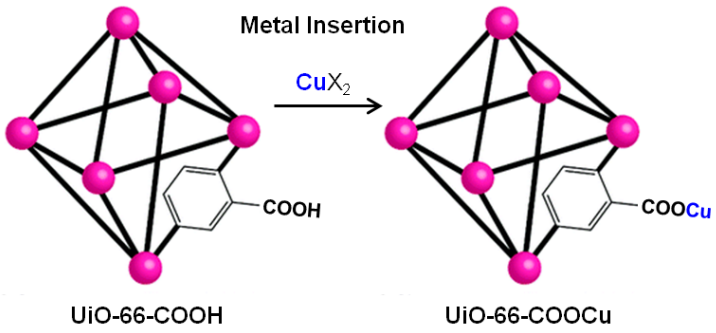

Figure 1. Illustration of metal insertion concept in UiO-66-COOH. Adapted from Lee et al.[41] with permission from The Royal Society of Chemistry.

The overall goal of this study was to synthesize UiO-66 versions functionalized with –COOCu groups and test their performance towards ammonia capture from air. Successful synthesis of this material will couple the desirable properties of Zr-BDC MOfs, such as robustness and high water stability, with the strong ammonia interaction sites of Cu-BTC. A material that has both these characteristics should be a promising candidate for air purification applications.

CHAPTER 2

MATERIALS AND EXPERIMENTAL METHODS

2.1 Materials and Synthesis Methods

Two different versions of UiO-66 were used in this study for the incorporation of metal carboxylate groups. The structure description for UiO-66 is as follows.

2.1.1 UiO-66 MOF Topology

UiO-66 is a zirconium (IV) based MOF with a highly stable $Zr_6O_4(OH)_4$ inorganic brick, where each Zr_6-octahedra is bound to twelve 1,2,4-benzenedicarboxylic acid (BDC) linkers.[34] Its 3D framework is made up of octahedral cages; each of them linked with 8 corner tetrahedral cages via triangular windows with 6 Å openings.[41] Several isostructural MOFs can be made by grafting different functional groups into the benzene dicarboxylate ligand. The crystal structure of UiO-66 is shown in Figure 2.

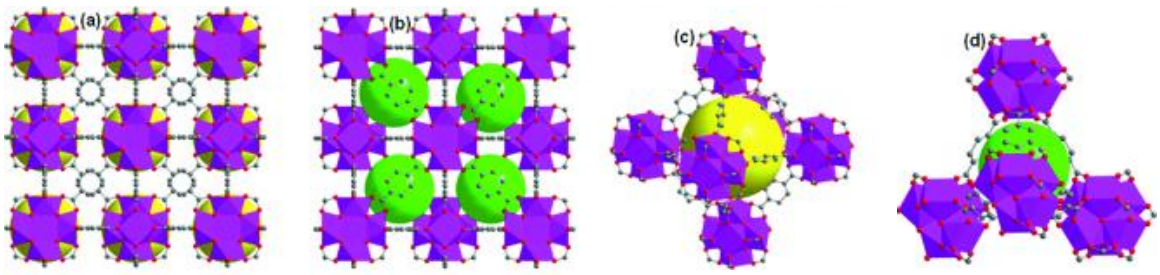

Figure 2. UiO-66 structural description. (a) Spatial arrangement of octrahedral cages. (b) Spatial arrangement of tetrahedral cages. (c) Single octahedral cage. (d) Single tetrahedral cage. Taken with permission from Biswas and Van der Voort.[41]

2.1.2 Synthesis Methods

All MOFs used for the purpose of this study were synthesized using known solvothermal methods previously published in literature. Some slight modifications were applied in some cases to obtain higher quality products and yields. All chemicals and solvents used in the synthesis were commercially available and used without further purification. Ligands used in the synthesis of UiO-66-COOH and UiO-66-$(COOH)_2$, are shown in Figure 3.

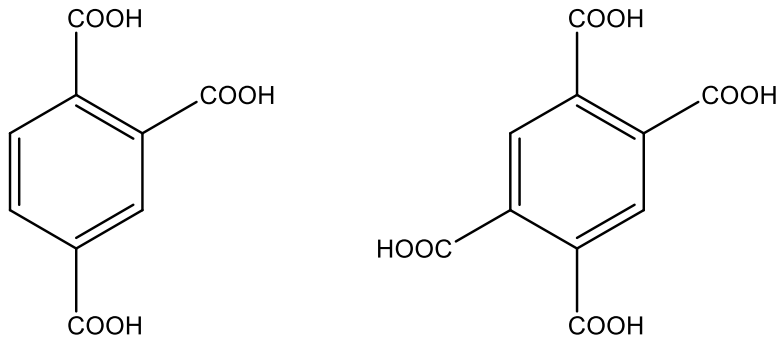

Figure 3. Functionalized terephthalate ligands used in the synthesis of UiO-66-X. Left: 1,2,4-benzenetricarboxylic acid (BDC-COOH). Right: 1,2,4,5-benzenetetracarboxylic acid (BDC-$(COOH)_2$).

2.1.2.1 UiO-66-COOH

Synthesis of this MOF was conducted in a similar fashion as reported by Biswas et al.[43] Zirconium oxynitrate hydrate (1.29 mmol, 300 mg), 1,2,4-Benzenetricarboxylic acid (2.58 mmol, 546 mg) and benzoic acid (38.82 mmol, 4.74 g) were dissolved in 9 mL of N,N-dimethylformamide (DMF). The reactant solution was transferred, without stirring, to a Teflon lined stainless steel reactor and heated in a programmable oven at 150 °C at a rate of 2.2 °C min^{-1}, held at this temperature for 24 h, then cooled at room

temperature. The resulting solid was filtered and washed three times with DMF, then, three times with methanol, and dried overnight under ambient conditions. The dried as-synthesized sample was activated by heating it at 65°C for 24 h under vacuum. In some cases, 0.38% (v/v) of water was added to the reactant mixture in order to obtain higher quality crystals.

2.1.2.2 UiO-66-$(COOH)_2$

UiO-66-$(COOH)_2$ was synthesized using a scaled-up version of the synthesis reported by Biswas et al.[42] Zirconyl chloride octahydrate (0.93 mmol, 300 mg) and 1,2,4,5-Benzenetetracarboxylic acid (0.93 mmol, 236.4 mg) were dissolved in 9.0 mL of N,N-dimethyacetamide (DMA) and 3.6 mL of formic acid. The reactant solution was transferred, without stirring, to a Teflon lined stainless steel reactor and heated in a programmable oven at 150 °C at a rate of 2.2 °C min^{-1}, held at this temperature for 24 h, then cooled at room temperature. The resulting solid was filtered and washed with DMF and acetone, followed by solvent exchange with methanol, and dried overnight under ambient conditions The dried as-synthesized sample was activated by heating it at 65°C for 12 h under vacuum.

2.2 Material Characterization Techniques

Structures of these MOFs were confirmed via Powder X-ray diffraction and Nitrogen Adsorption Measurements. Elemental analysis was conducted using Inductively Coupled Plasma Emission Spectroscopy and X-Ray Photoelectron Spectroscopy.

2.2.1 Powder X-ray diffraction (PXRD)

X-ray diffraction patterns of the powder samples were obtained with a X'Pert Pro PANanalytical X-ray diffractometer using Cu Kα (λ= 1.542 Å) radiation at room temperature, with a step size of 2θ= 0.02° over the 2θ range of 5-50 degrees. PXRD patterns of the as-synthesized and activated samples were compared with patterns from simulated data to test the impact of activation and addition of functional groups on the crystal structure.

2.2.2 Thermal Gravimetric Analysis (TGA)

Thermal gravimetric analysis was performed using a Netzsch STA 449 F1 Jupiter instrument to study the dehydration, desolvation and decomposition of the materials. Approximately 10-30 mg of sample were heated from 20-800°C at a constant heating rate of 2 K min^{-1} under air flow (20 mL min^{-1}).

2.2.3 Nitrogen Adsorption Isotherm Measurements

Nitrogen adsorption isotherms were measured at 77 K (-196°C) using a Quadrasorb system from Quantrachrome Instruments, in order to calculate the specific surface area and total pore volume of the materials. Approximately 50-100 mg of the activated samples were used to collect the isotherms. The specific surface area of the

materials was calculated by fitting the nitrogen adsorption data to the Brunauer, Emmett, and Teller (BET) model over the pressure range $P/P_o < 0.05$ as suggested by Walton et al.[44] Although the BET model is defined for multi-layer adsorption, and adsorption in MOFs can be better described through a pore filling mechanism, the model can still be applied by choosing the appropriate pressure range ($0.005< P/P_o < 0.03$).

2.2.4 Inductively Coupled Plasma Optical Emission Spectrometry (ICP-OES)

Samples were shipped after metal insertion to ALS Environmental for elemental analysis via Inductively Coupled Plasma (ICP) Optical Emission Spectrometry in order to determine the Zr and Cu content of the materials.

2.2.5 X-Ray Photoelectron Spectroscopy (XPS)

The oxidation state of copper was determined by XPS. Data was collected using a Thermo K- Alpha photoelectron spectrophotometer with an Al Kα source. Analysis was a point scan with a 50um radius spot size.

2.3 Water Vapor Adsorption Isotherm Measurements

Water vapor adsorption isotherms were collected using an Intelligent Gravimetric Analyzer (IGA-3) apparatus from Hiden Isochema, at 25°C and 1 bar. Prior to the runs, samples were activated in situ until no weight loss was observed. Experiments were conducted up to 90% RH to avoid water condensation using dry air as the carrier gas. Total gas flow rate was set at 200 cm^3 min^{-1}. Two mass flow controllers were used to vary the ratio of saturated air to dry air in order to control the desired relative humidity.

2.4 Adsorber Dynamics: Breakthrough curves

In order to test the performance of the materials for ammonia adsorption under dynamic conditions, breakthrough studies were performed using a lab-built microbreakthrough system. In a common breakthrough experiment, a column packed with the material of interest (adsorbent) is challenged to a gas stream of the desired adsorbate (in this case, ammonia). Once the bed is saturated, the adsorbate breaks through and is detected at the outlet of the bed. By measuring the concentration of the gas at the outlet of the adsorption column through time, a breakthrough curve is obtained.

Ammonia breakthrough experiments were conducted under dry (0% RH) and humid conditions (80% RH) at room temperature using an apparatus as shown in Figure 4. For dry breakthrough runs, an MFC is used to control the ammonia (with a feed concentration of 1500 ppm in air) flow rate at 20 mL min^{-1}. For wet runs, air at 16 mL min^{-1} is passed through a H_2O bubbler and then combined with an ammonia stream at 4 mL min^{-1}. The ammonia concentration at the bed outlet is monitored continuously using an electrochemical sensor.

The samples were activated in situ for 2 h under nitrogen flow at their respective activation temperatures prior to testing. A quartz bed with a diameter of 4 mm was used as the adsorption column, and approximately 5-30 mg of sample was used to pack the column up to 4.3 mm in height (for a final standardized volume of 55 mm^3). Once the ammonia effluent concentration reaches 500 ppm, the system is switched to a nitrogen stream at 50 mL min^{-1} in order to preserve the life of the sensor and start the desorption step.

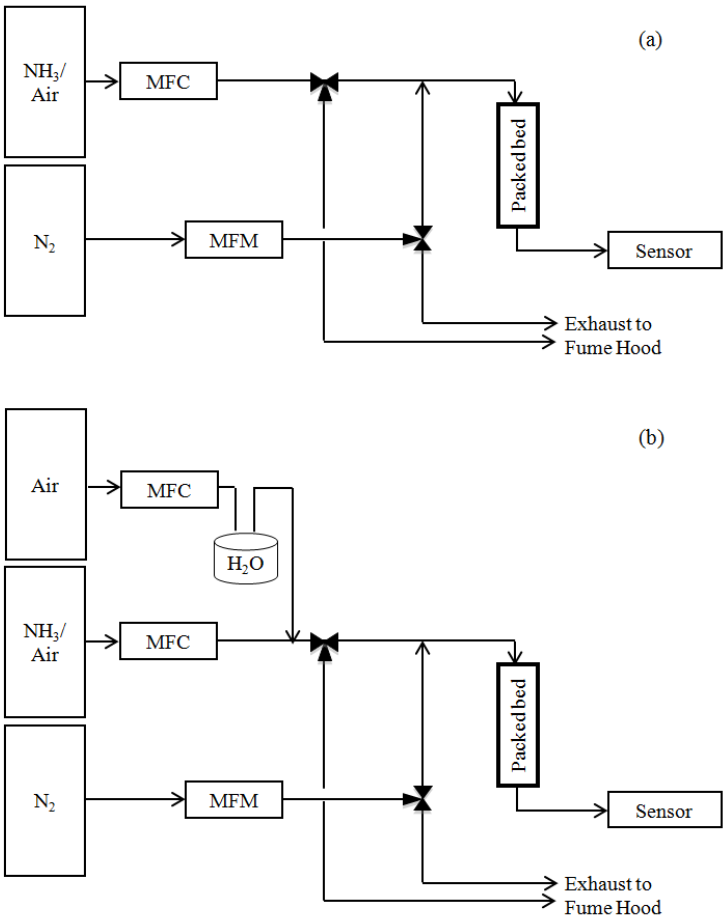

Figure 4. Schematic of ammonia breakthrough system (a) dry conditions (b) humid conditions.

CHAPTER 3

RESULTS AND DISCUSSION

3.1 Materials Synthesis and Characterization

Two different batches of UiO-66-COOH were synthesized for this study. At first, 5 batches of UiO-66-COOH (UiO-66-COOH_S1) with an average BET surface area of 855±104 m^2 g^{-1} were synthesized. Nitrogen physisorption data was collected with a Micromeritics Gemini VII instrument at the low-pressure region of $0.005<P/P_o<0.03$ as detailed in Section 2.3. Although this value is consistent with experimental results published by Biswas et al.,[43] it is higher than the theoretical value of 551 m^2 g^{-1} reported by Yang et al.[45] It is hypothesized that this increase in surface area may be due to defects present in the as-synthesized materials, such as missing linkers or others. Additional batches of UiO-66-COOH were later synthesized, but comparable surface area values could not be obtained. For subsequent batches (UiO-66-COOH_S2), water was added to the reaction mixture to obtain a higher quality product with an average surface area of 658±20 m^2 g^{-1}. UiO-66-COOH_S2 N_2 adsorption data was collected with a Quantachrome Quadrasorb apparatus.

UiO-66-$(COOH)_2$ with a BET surface area of 320 m^2 g^{-1} was also synthesized for this work. Comparison between the PXRD patterns of the as-synthesized materials with the simulated pattern of UiO-66 shows that all the materials belong to the same isostructural family (Figure 5).

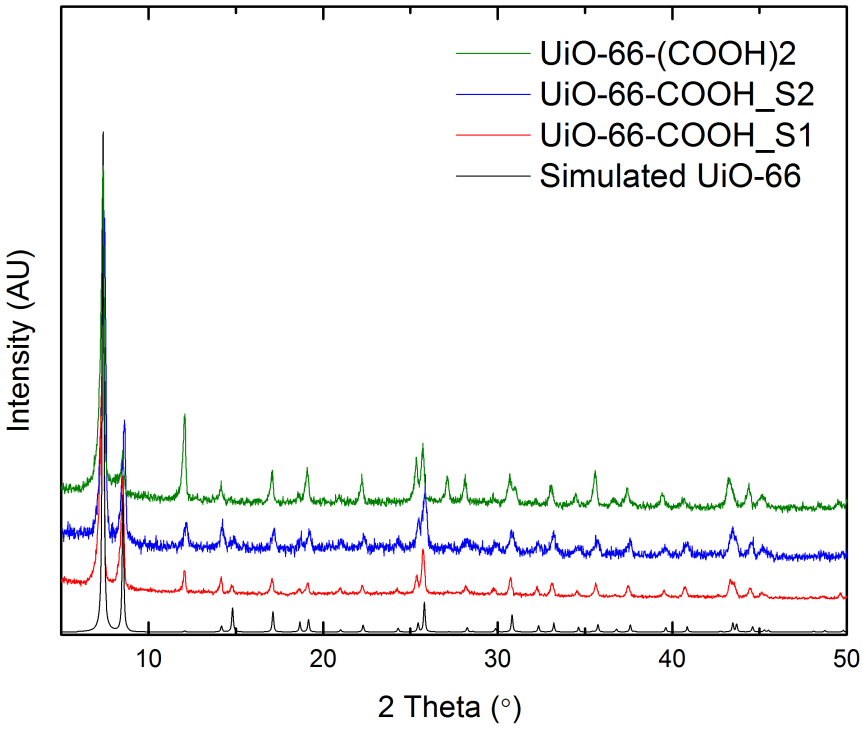

Figure 5. Comparison between PXRD patterns of as-synthesized UiO-66-COOH and UiO-66-$(COOH)_2$, and the theoretical pattern of UiO-66.

N_2 adsorption isotherms for all materials and their respective calculated surface areas are shown in Figure 6 and Table 1, respectively. As expected, the surface area and pore volume of UiO-66-COOH and UiO-66-$(COOH)_2$ is reduced significantly when compared to the theoretical UiO-66 surface area due to the inclusion of the carboxylic acid groups.

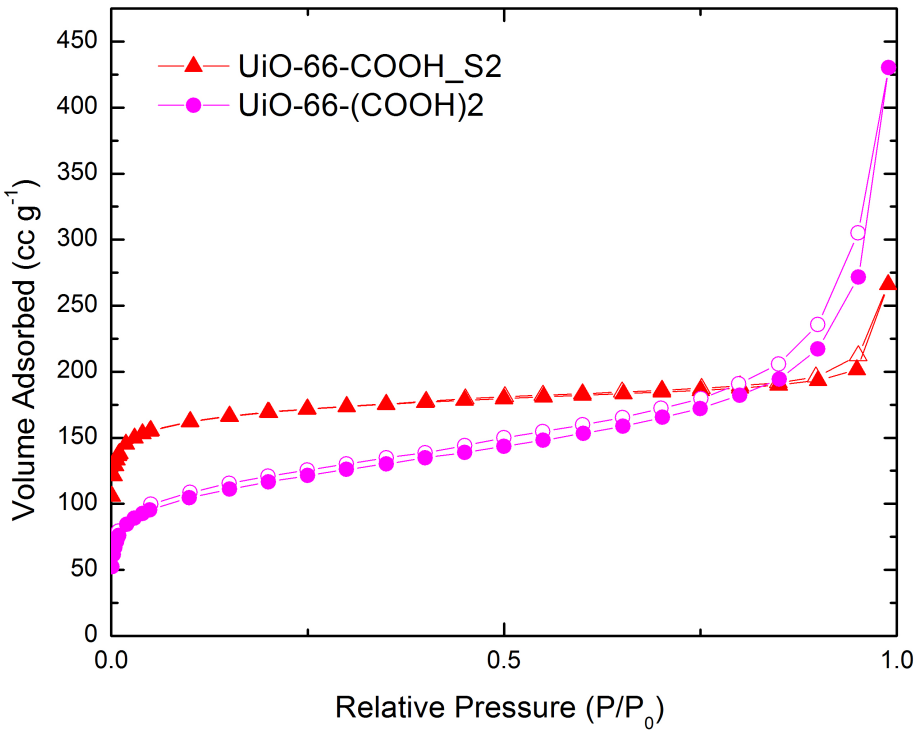

Figure 6. Nitrogen adsorption isotherms of MOFs used in this work (closed symbols - adsorption, open symbols – desorption).

Table 1. Comparison of textural properties of MOFs used in this work.

MOF	BET Surface Area ($m^2\ g^{-1}$)	Total pore volume[a] ($cm^3\ g^{-1}$)
UiO-66[b]	1186	0.42
UiO-66-COOH_S1	855	-
UiO-66-COOH_S2	658	0.28
UiO-66-$(COOH)_2$	364	0.22

[a]Measured at P/P_0=0.5.
[b]Theoretical values reported from literature.[46]

3.2 Study of Metal Insertion on MOFs with Uncoordinated Carboxylic Acid Groups

In order to study the effect of solvent, counter anion and temperature on metal (Cu) loading, various reactions were conducted with UiO-66-COOH. Copper loading was determined by ICP-OES as detailed in Section 2.3.4. Once the parameters were optimized, a post synthetic modification was performed on all materials (UiO-66-COOH, UiO-66-$(COOH)_2$) to insert copper atoms into the frameworks. Metalated samples are referred as UiO-66-COOCu and UiO-66-$(COOCu)_2$ for metal insertions on UiO-66-COOH and UiO-66-$(COOH)_2$, respectively.

3.2.1 Solvent Effect on Metal Loading and Material Properties

The effect of solvent on metal loading and surface area was investigated by conducting various metal insertion reactions with different solvents. Methanol (CH_3OH), water (H_2O) and N,N-dimethylformamide (DMF) were chosen for the study due to their different sizes (Table 2). Approximately 30 mg of activated material (UiO-66-COOH_S1) were soaked in 0.1 M solutions of $Cu(NO_3)_2 \cdot 3H_2O$ in 10 mL of the respective solvent (for a resulting 0.3 mg MOF per mL of solution), and left without stirring for 5 h. Reactions were carried out at room temperature (RT). After the metal insertion, all samples were washed with methanol (the samples dissolved in DMF were washed with DMF before methanol), and left to dry overnight.

Table 2. Kinetic diameter of solvents used for metal insertion.

Molecule	Kinetic diameter (Å)[a]
DMF	~5.5
CH_3OH	3.8-4.1
H_2O	2.6

[a]Data reported from literature.[47]

Materials were activated for 24 h at 65°C under vacuum prior to ICP-OES analysis. Copper loading measurements are detailed in Table 3. A trend can be observed with respect to the size of the solvent, being the reaction with the smallest solvent (H_2O) the one that resulted in the highest metal loading. These results are consistent with results published by Meng et al.[40] where it was hypothesized that the size of the solvent may limit the entry of metal ions into the frameworks. The pore size of UiO-66-COOH should be less than 6 Å, which is the reported pore diameter of the parent UiO-66 and the inclusion of carboxylic acid groups into the framework should cause partial pore blocking. Although it was expected that the sample with the highest copper loading may exhibit the highest loss in surface area, this was not the case. Sample 3 had a surface area loss of 7% when compared to the surface area of UiO-66-COOH_S1. This fact may be attributed to an insufficient activation of the material. PXRD patterns were collected for all samples and compared to the theoretical pattern of UiO-66 and the pattern of as-synthesized UiO-66-COOH_S1 (Figure 7). It is evident that the patterns remained virtually unaltered by the metal insertion procedure.

Table 3. Solvent effect on metal loading results.

Sample	Metal salt	Solvent	BET Surface Area (m^2 g^{-1})	Copper Loading (Cu/Zr Mass Ratio)
1	$Cu(NO_3)_2 \cdot 3H_2O$	DMF	575	0.013
2	$Cu(NO_3)_2 \cdot 3H_2O$	CH_3OH	781	0.019
3	$Cu(NO_3)_2 \cdot 3H_2O$	H_2O	794	0.052

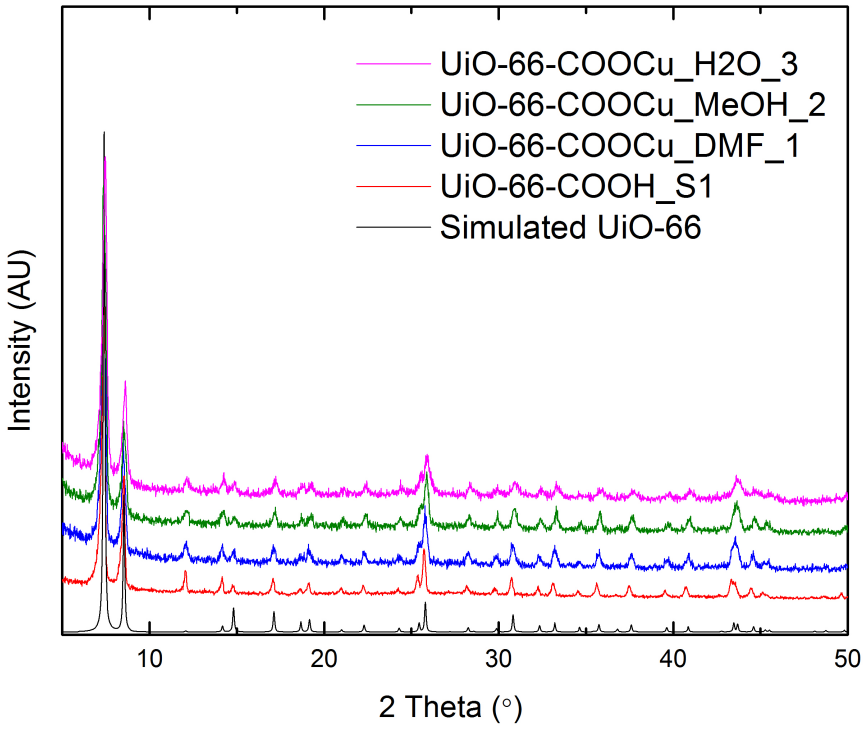

Figure 7. Comparison between PXRD patterns of metalated samples from solvent effect study and theoretical pattern of UiO-66 and as-synthesized UiO-66-COOH_S1.

It is hypothesized that such low metal loadings may be due to a partial metalation of the framework, where only the carboxylic acid groups pointing outwards of the surface are coordinated to copper ions. In order to decrease the mass transfer limitations during the metal insertion, further experiments were carried out by increasing the ratio of desolvated MOF to the volume of the $Cu(NO_3)_2$ solution (mg MOF per mL of copper solution), and by stirring the reaction mixture. Reactions were conducted in a similar fashion as before: approximately 190 mg of activated material (UiO-66-COOH_S1) were soaked in 0.1 M solutions of $Cu(NO_3)_2 \cdot 3H_2O$ in 25 mL of the respective solvent (for a resulting 7.6 mg MOF per mL of solution), and left stirring for 5 h. Reactions were carried out at room temperature (RT). After the metal insertion, all samples were washed with methanol (the samples dissolved in DMF were washed with DMF before methanol), and left to dry overnight.

Although still low loadings were obtained, the copper loading was increased for all samples (Table 4), especially in the case of DMF. PXRD patterns for all metalated samples were compared to the theoretical pattern of UiO-66 and the pattern of as-synthesized UiO-66-COOH_S1. Figure 8 confirms that all samples belong to the same isostructural family. This increase in copper loading with increase in concentration may be due to higher interactions and a higher contact area between MOF particles and the metal salt solution.

Table 4. Solvent effect on metal loading with increasing MOF concentration.

Sample	Metal salt	Solvent	BET Surface Area (m^2 g^{-1})	Copper Loading (Cu/Zr Mass Ratio)
4	$Cu(NO_3)_2 \cdot 3H_2O$	DMF	498	0.230
5	$Cu(NO_3)_2 \cdot 3H_2O$	CH_3OH	739	0.042
6	$Cu(NO_3)_2 \cdot 3H_2O$	H_2O	720	0.059

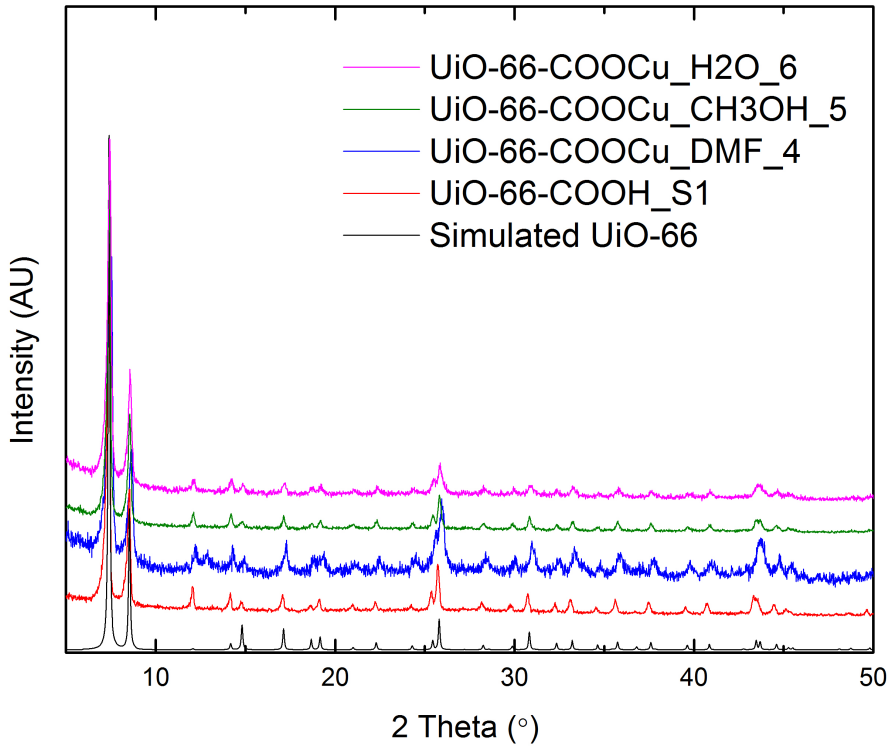

Figure 8. Comparison between PXRD patterns of metalated samples from concentration effect study and theoretical pattern of UiO-66 and as-synthesized UiO-66-COOH_S1.

3.2.2 Counter Anion Effect on Metal Loading and Material Properties

The coordination nature of counter anions has been found to have an effect on the catalytic performance of various metal salts.[48,49] Moreover, Valvekens et al.[48] found that copper counter anions have an effect on the copper loading of copper ions immobilized in MOFs such as MOF-253. To test the effect of the charge compensating anion on the copper loading and physical properties of UiO-66-COOCu, different experiments were conducted using different metal salts. For each case, approximately 30 mg of activated material (UiO-66-COOH_S1) were soaked in 0.1 M solutions of the respective copper salt [$CuCl_2 \cdot 2H_2O$, $Cu(NO_3)_2 \cdot 3H_2O$ or $Cu(BF_4)_2 \cdot 6H_2O$] in 10 mL of DMF (for a resulting 0.3 mg MOF per mL of solution), and left without stirring for 5 h. Reactions were carried out at room temperature (RT). After the metal insertion, all samples were washed with DMF and methanol and left to dry overnight. From results shown in Table 5, it is evident that the counter anion has an effect on the copper loading, although not as significant as the effect due to different solvents. The copper loading increases inversely with the coordination nature (strength with which the counter anion binds to the copper ion) of the anions. PXRD patterns of the metalated samples were collected and compared to the as-synthesized pattern of UiO-66-COOH_S1 and the simulated pattern of UiO-66 to ensure no changes were introduced by the metal insertion (Figure 9).

Table 5. Counter anion effect on metal loading results.

Sample	Metal salt	Solvent	BET Surface Area (m^2 g^{-1})	Copper Loading (Cu/Zr Mass Ratio)
1	$CuCl_2 \cdot 2H_2O$	DMF	614	0.004
2	$Cu(NO_3)_2 \cdot 3H_2O$	DMF	575	0.013
3	$Cu(BF_4)_2 \cdot 6H_2O$	DMF	652	0.031

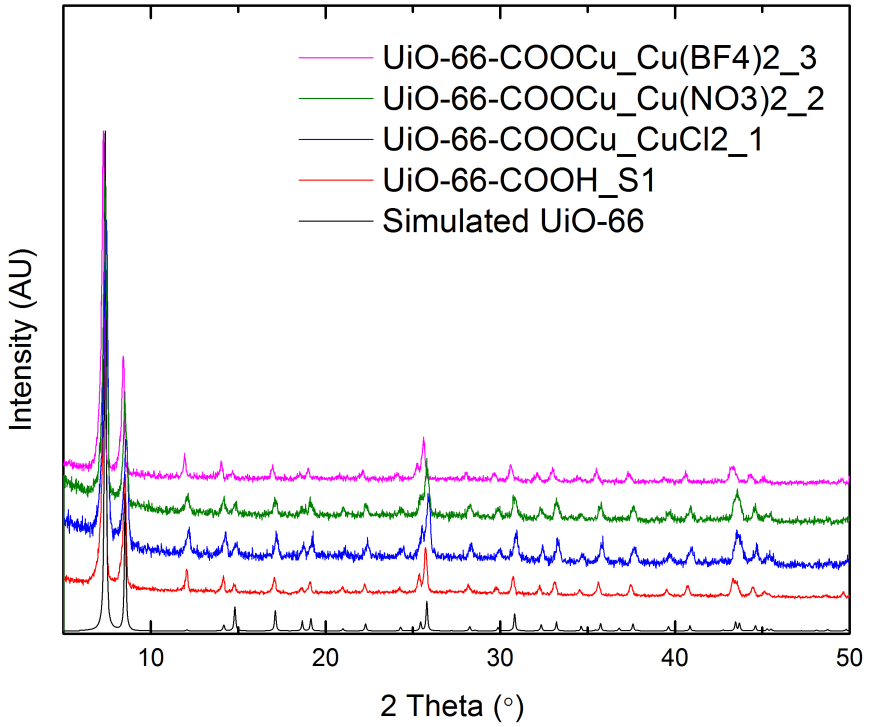

Figure 9. Comparison between PXRD patterns of metalated samples from counter anion effect study and theoretical pattern of UiO-66 and as-synthesized UiO-66-COOH_S1.

Although from the counter anions included in this study, $Cu(BF_4)_2$ was determined to be the best option to obtain higher copper loadings, further experiments with UiO-66-$(COOH)_2$ showed that the most adequate counter anion was $Cu(NO_3)_2$.

Differences obtained for both materials may be due to the fact that the pores of UiO-66-$(COOH)_2$ are more restricted due to the inclusion of more bulky groups (-COOH) and therefore, the size of the counter anions may restrict the entry of metal ions into the framework even more.

3.2.3 Kinetic Effects on Metal Loading and Material Properties

In order to account for any kinetic limitations occurring during the metal insertion, a reaction was conducted at a higher temperature for a longer period of time. Reactions were carried out at 65°C for 24 h, similar to the experimental procedure published by Bloch et al.[50] in which copper and palladium metals were grafted into the open bipyridine ligand sites of MOF-253. Similar to previous reactions, approximately 30 mg of activated material (UiO-66-COOH_S1) were soaked in 10 mL of a 0.1 M solution of $Cu(NO_3)_2 \cdot 3H_2O$ in DMF (for a resulting 0.3 mg MOF per mL of solution), and left stirring for 24 h at 65°C in an oil bath. After the metal insertion, all samples were washed with DMF and methanol and left to dry overnight.

Elemental analysis results (Table 6) shows that the copper loading increases by a factor of ~5 when the reaction time and temperature are increased. These results show that there are some kinetic limitations related to the insertion of copper atoms into the framework, which can be minimized by increasing the reaction time. Further experiments were carried out using $CuCl_2$ as the counter anion, and similar results were obtained (copper loading was also increased by a factor of ~5). PXRD patterns of the materials (Figure 10) were compared to the theoretical pattern of UiO-66 and to the parent material UiO-66-COOH_S1 to ensure the materials were not affected by the metal insertion procedure.

Table 6. Temperature and time effect on metal loading results.

Sample	Metal salt/Solvent	Temperature/ Time	BET Surface Area (m^2 g^{-1})	Copper Loading (Cu/Zr Mass Ratio)
1	$Cu(NO_3)_2 \cdot 3H_2O$/DMF	RT/ 5 h	575	0.013
2	$Cu(NO_3)_2 \cdot 3H_2O$/DMF	65°C/ 24 h	506	0.064

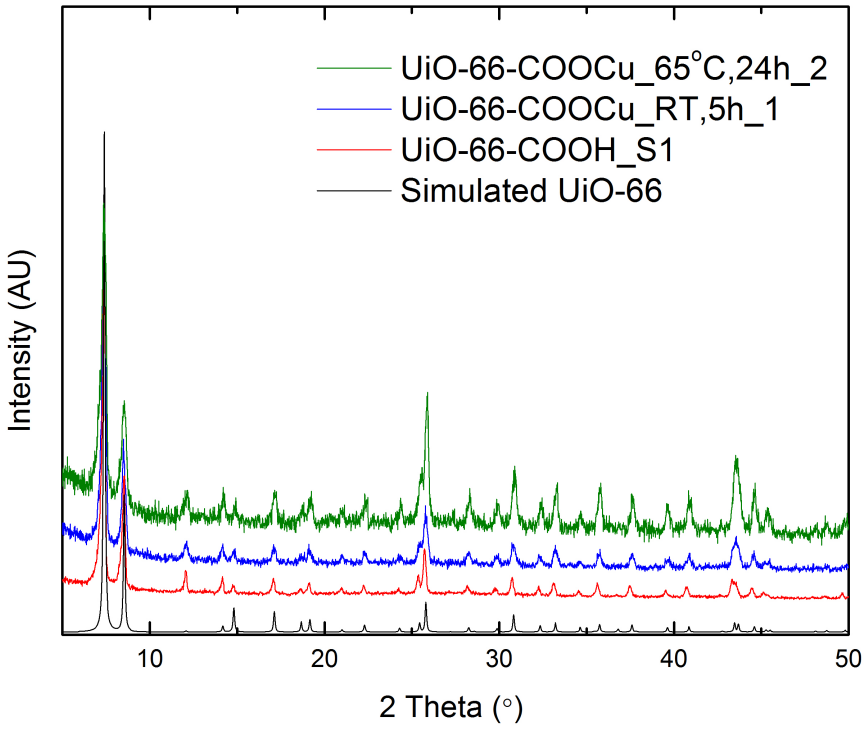

Figure 10. Comparison between PXRD patterns of metalated samples from kinetic limitations study and theoretical pattern of UiO-66 and as-synthesized UiO-66-COOH_S1.

3.2.4 Post Synthetic Modification of UiO-66-COOH and UiO-66-$(COOH)_2$

After all parameters affecting the metal insertion were optimized, a post-synthetic modification of UiO-66-COOH and UiO-66-$(COOH)_2$ was conducted in order to deliver the final UiO-66-COOCu and UiO-66-$(COOCu)_2$ materials. Copper complexation was attained as follows: approximately 190 mg of activated material [UiO-66-COOH_S2 or UiO-66-$(COOH)_2$] were soaked in 25 mL of a 0.1 M solution of $Cu(NO_3)_2 \cdot 3H_2O$ in DMF (for a resulting 7.6 mg MOF per mL of solution). The reaction mixture was left stirring for 24 h at 65°C in an oil bath. After the metal insertion, all samples were washed with DMF and methanol and left to dry overnight. A clear indication that the copper complexation had occurred is the powder color change from white to blue.

3.2.4.1 Powder X-Ray Diffraction

PXRD data (Figure 11) show UiO-66-COOCu and UiO-66-$(COOCu)_2$ to be isostructural with UiO-66. Comparison between samples before and after metalation proves the materials are not affected by the metal insertion.

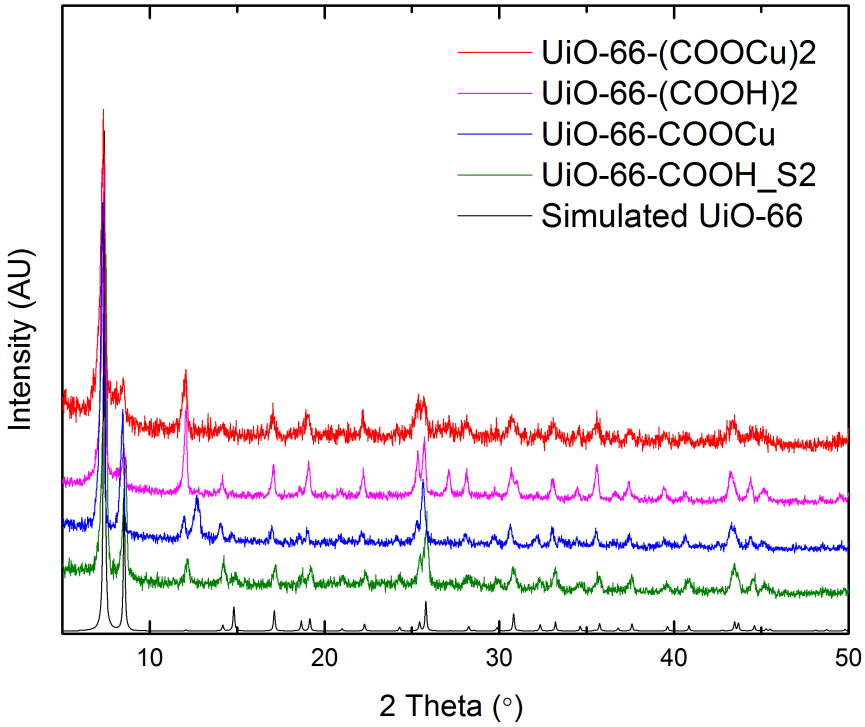

Figure 11. Comparison between PXRD patterns of samples before and after metalation, and theoretical pattern of UiO-66.

3.2.4.2 Nitrogen Isotherm Measurements

Nitrogen adsorption isotherms were collected to study the effect of copper insertion on the textural properties of UiO-66-COOH and UiO-66-$(COOH)_2$. Figure 12 shows the nitrogen isotherms for UiO-66-COOH, UiO-66-COOCu, UiO-66-$(COOH)_2$ and UiO-66-$(COOCu)_2$. Samples were activated prior to analysis according to their activation conditions as detailed in Table 7.

Table 7. Activation conditions for metalated samples.

MOF	Activation Process (under vacuum)
UiO-66-COOCu	65°C (24 h)
UiO-66-$(COOCu)_2$	65°C (12h)

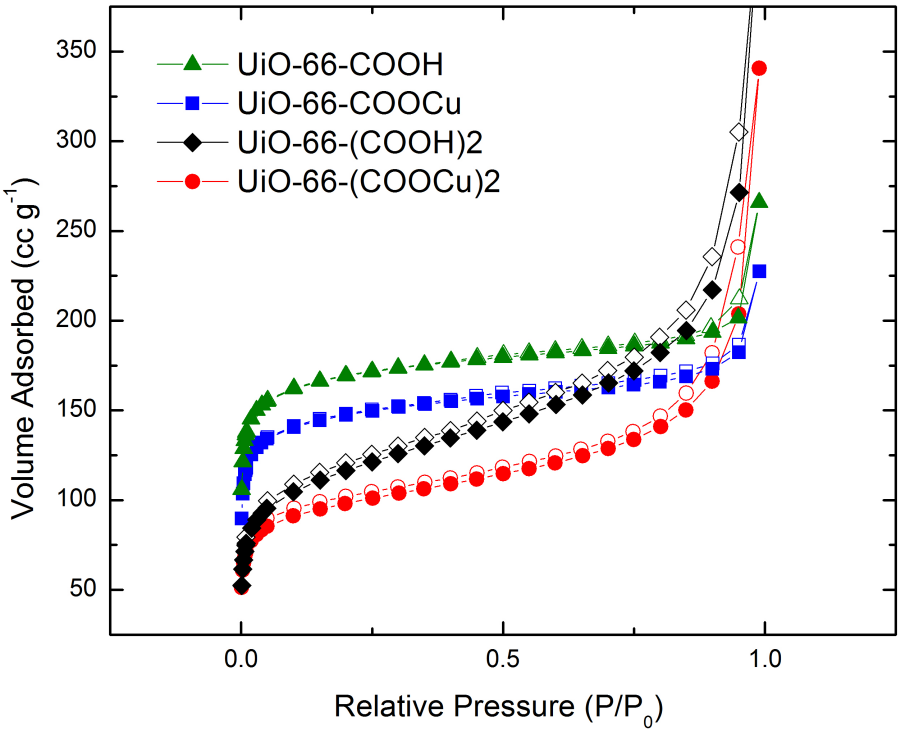

Figure 12. Nitrogen adsorption isotherms illustrating the effect of copper insertion on the nitrogen uptake of UiO-66-COOH and UiO-66-$(COOH)_2$ (closed symbols - adsorption, open symbols – desorption).

Nitrogen uptake is reduced after the insertion of copper atoms into the frameworks, probably due to a higher framework density and partial pore blocking caused by the introduction of the copper carboxylate groups. This can be further confirmed by the decrease in surface area and pore volume as listed in Table 8.

Table 8. Textural properties of materials before and after metal insertion.

MOF	BET Surface Area ($m^2\ g^{-1}$)	Total Pore Volume[a] ($cm^3\ g^{-1}$)
UiO-66-COOH_S2	658	0.28
UiO-66-COOCu	564	0.24
UiO-66-$(COOH)_2$	364	0.22
UiO-66-$(COOCu)_2$	357	0.18

[a]Measured at P/P_0=0.5.

3.2.4.3 Thermo-gravimetric Analysis (TGA)

The thermal stability of the metal loaded samples (after activation, Table 7) was analyzed by TGA. Figure 13 shows that both UiO-66-COOCu and UiO-66-$(COOCu)_2$ decompose at approximately 220°C, which is less than the observed decomposition temperatures for UiO-66-COOH and UiO-66-$(COOH)_2$. UiO-66-COOH is thermally stable up to 340°C, consistent with results reported by Biswas et al.[43] and UiO-66-$(COOH)_2$ is thermally stable up to 300°C, similar to the previously reported decomposition temperature (290°C).[42] Although the reason for this decrease in thermal stability is still unclear, this behavior has also been observed for other UiO-66 versions.[42-43,51-52] Below the decomposition temperature, all the activated

materials display one weight loss step corresponding to the removal of adsorbed water molecules.

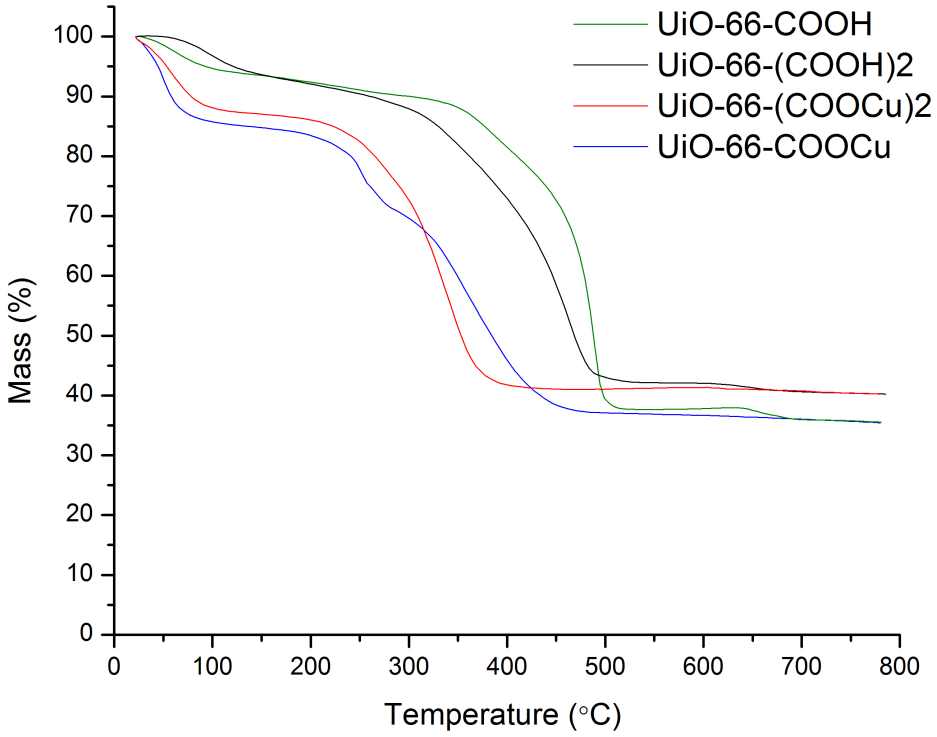

Figure 13. TGA curves of activated UiO-66-COOH, UiO-66-$(COOH)_2$, UiO-66-$(COOCu)_2$ and UiO-66-COOCu.

3.2.4.4 Copper Loading

The copper loading of metalated samples was determined by ICP analysis, as summarized in Table 9. Although samples were activated before ICP analysis, the re-adsorption of water into the pores of the frameworks may cause inconsistencies in the results, if normalized by total mass of material. To avoid this, results are presented as the mass ratio of copper to zirconium (Cu/Zr Mass Ratio).

Lower copper loadings were obtained for UiO-66-$(COOCu)_2$ than for UiO-66-COOCu, even when there are more chelating units (uncoordinated carboxylic acid groups) in the UiO-66-$(COOH)_2$ framework (2 free carboxylic acid groups per unit cell). This is probably due to the fact that the entry of metal ions into the UiO-66-$(COOH)_2$ framework is more restricted because of its lower pore space (due to the presence of dicarboxylic acid groups).

Even though the parameters chosen for the metal insertion procedure hindered higher copper loadings than the ones obtained in previous experiments, these are still far from the theoretical Cu to Zr mass ratios of 0.697 and 1.393, for UiO-66-COOCu and UiO-66-$(COOCu)_2$, respectively. These results imply that there are still some mass transfer limitations associated with the incorporation of metal ions into frameworks with low pore sizes such as UiO-66-COOCu and UiO-66-$(COOCu)_2$. It is hypothesized that due to the inaccessibility of the UiO-66-$(COOH)_2$ cages, only the carboxylic acid groups on the surface of the MOF crystal undergo coordination with the copper ions.

Table 9. Copper loadings in UiO-66-COOCu and UiO-66-$(COOCu)_2$.

MOF	Copper Loading (Cu/Zr Mass ratio)
UiO-66-COOCu	0.38
UiO-66-$(COOCu)_2$	0.12

3.2.4.5 X-ray Photoelectron Spectroscopy

The chemical oxidation state of the metalated samples was determined by XPS analysis. Figure 14 and Figure 15 show the XPS spectrum (each spectrum is an average of 10 scans) for UiO-66-COOCu and UiO-66-$(COOCu)_2$, respectively. The strong presence of a satellite peak around 943 eV, in both spectra, is a clear indication of the existence of Cu^{2+}. This satellite peak, is characteristic of CuO, whereas Cu_2O and elemental Cu lacks this feature.[53-55] Satellite peaks appear due to a loss in electron kinetic energy during the photoemission. Other peaks at approximately, 956 and 936 eV correspond to the Cu $2p_{1/2}$ and Cu $2p_{3/2}$ levels, respectively.

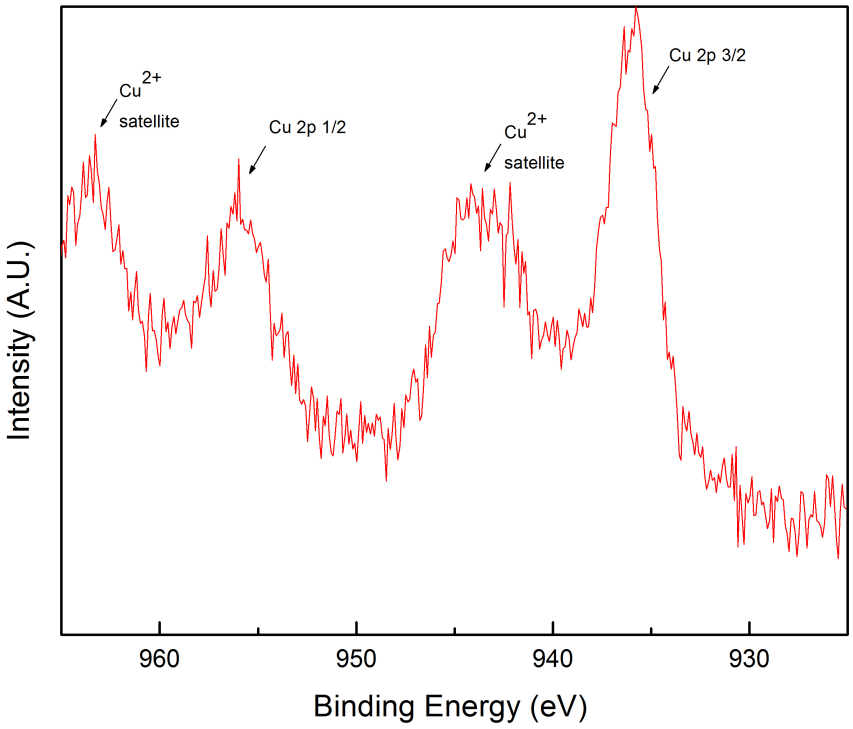

Figure 14. XPS spectrum of Cu 2p level for UiO-66-COOCu.

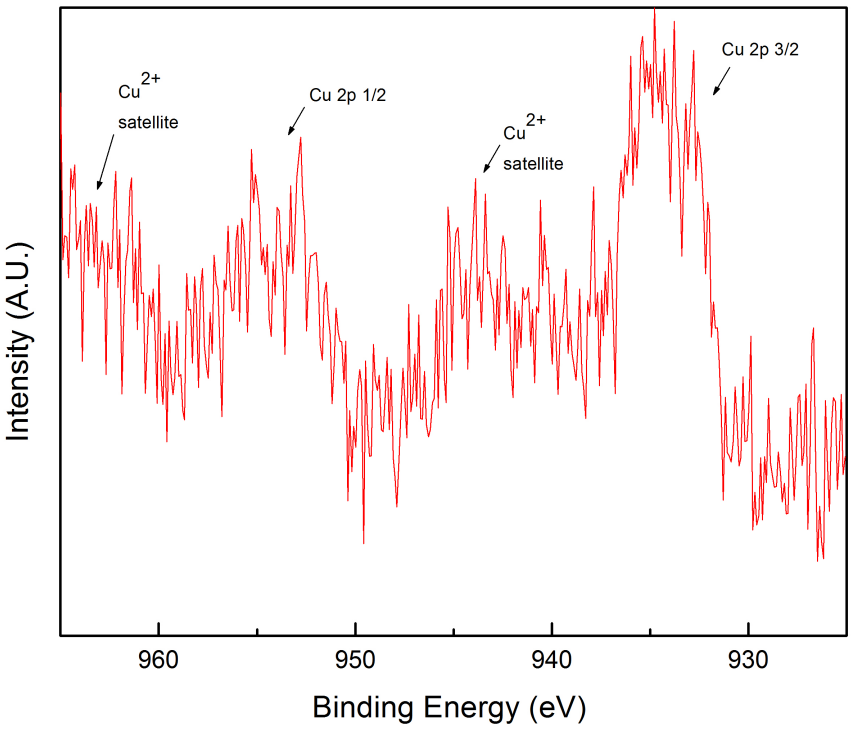

Figure 15. XPS spectrum of Cu 2p level for UiO-66-$(COOCu)_2$.

3.2.4.6 Water Vapor Adsorption Isotherm Measurements

In order to confirm the water stability of the materials, water vapor adsorption measurements where collected at 25°C and 1 bar. Figure 16 shows water adsorption and desorption isotherms for the metal-loaded samples, UiO-66-COOCu and UiO-66-$(COOCu)_2$. Both MOFs exhibit a steep rise of water vapor loadings at low relative humidities, indicative of a Type I isotherm. Although water vapor adsorption data wasn't collected in this study for the non-metalated MOFs, UiO-66-COOH and UiO-66-$(COOH)_2$, a good comparison can be made with previous studies on the effect of functional groups on the water vapor adsorption of UiO-66. Experimental results reported by Hu et al.[56] show that UiO-66-$(COOH)_2$ also exhibits high loadings at the low pressure

region due to water interference, when compared to other functionalized UiO-66 versions, such as $–NH_2$, $-(OH)_2$, $-F_4$ and $–(OCH_2CH_3)_2$. MOFs with open metal sites have also been found to exhibit Type I isotherms due to the affinity of the metal cations toward water.[57] It is important to note that even though, the metalated samples exhibit a behavior similar to MOFs with coordinatively unsaturated metal centers, the materials presented here have lower water vapor loadings than these.

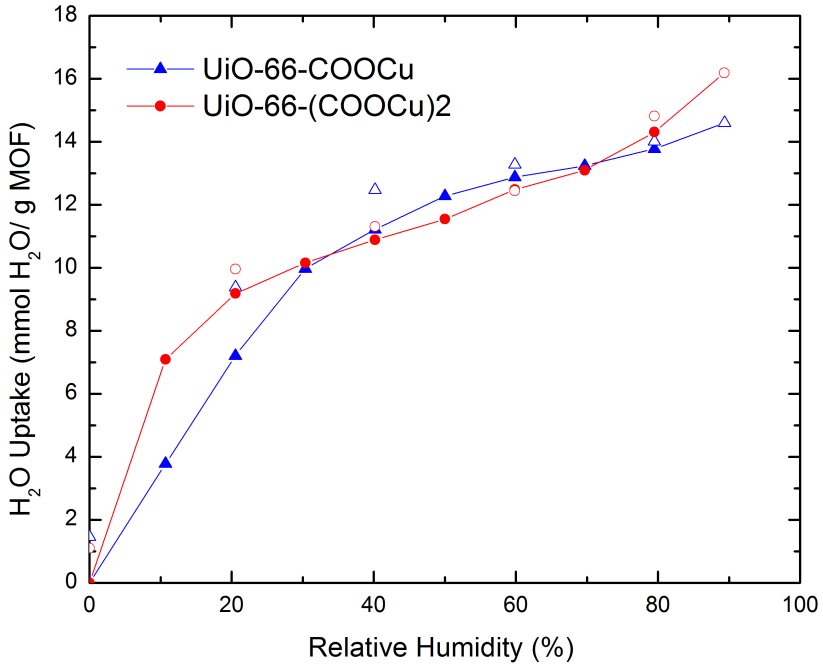

Figure 16. Water vapor sorption/desorption isotherms at 25°C and 1 bar for UiO-66-COOCu and UiO-66-$(COOCu)_2$ (closed symbols- adsorption, open symbols– desorption).

The desorption isotherms of the metal loaded MOFs exhibit low hysteresis with a portion of water being retained upon desorption. At 0% RH, UiO-66-COOCu and UiO-66-$(COOCu)_2$ retain 1.46 mmol g^{-1} and 1.10 mmol g^{-1}, respectively. Confirmation of the water stability of the materials is presented by the BET surface area analysis of the samples (Table 10). Samples were regenerated before N_2 physisorption studies. No

apparent loss in surface area was observed for the materials, suggesting they are both water stable. Although it has been proven that isotherm character alone is not sufficient to determine the water stability of MOFs,[51] PXRD patterns of the samples after the water vapor adsorption experiments were not collected at the time.

Table 10. BET surface area analysis before and after water exposure.

MOF	Loading, 90% RH ($cm^3\ g^{-1}$)	BET Surface Area ($m^2\ g^{-1}$)		
		Before	After	% Loss
UiO-66-COOCu	0.28	564	634	0
UiO-66-$(COOCu)_2$	0.31	357	394	0

3.3 Ammonia Breakthrough Measurements

Ammonia breakthrough measurements were conducted under dry (0% RH) and wet conditions (80% RH) for UiO-66-COOCu and UiO-66-$(COOCu)_2$. Previously activated samples were reactivated for 2 h at 65°C under N_2 flow prior to runs. Results were normalized on a per mass basis, as the bed volume was kept constant at 55 mm^3 for all runs. Repeatability of normalized breakthrough time for these experiments was +/- 12%. The ammonia dynamic capacities were calculated using Equation (1):

$$W_E = \frac{\dot{n}_{NH_3} t_b}{m_a} \tag{1}$$

where,

W_E= NH_3 dynamic capacity

t_b= breakthrough time (defined as the time needed for [NH_3]= 50 ppm)

$\dot{n}_{NH_3}$= NH_3 molar flow rate adsorbed by the bed until t_b

m_a= adsorbent activated mass

Ammonia breakthrough experiments were also conducted for UiO-66-COOH in order to compare the NH_3 dynamic capacities of the materials before and after the introduction of the copper carboxylate groups. UiO-66-COOH breakthrough curves for dry and wet conditions are presented in Appendix A. It is important to note that the NH_3 dynamic capacity for UiO-66-$(COOH)_2$ presented in Table 11 is a previously reported experimental value[26] and represents the loading until full saturation. In contrast with the results presented here, this NH_3 uptake was calculated by integrating the NH_3 breakthrough curve until saturation (C/C_o=1).

Dry and wet NH_3 breakthrough curves for UiO-66-COOCu and UiO-66-$(COOCu)_2$ are shown in Figure 17 and Figure 18, respectively. As it can be seen below, UiO-66-$(COOCu)_2$ performs better (longer breakthrough time) than UiO-66-COOCu under both, dry and wet, conditions. Under dry conditions UiO-66-COOCu and UiO-66-$(COOCu)_2$ had breakthrough times of 2267 min g^{-1} and 4764 min g^{-1}, respectively. Breakthrough times for wet conditions were 2318 min g^{-1} and 5107 min g^{-1}, for UiO-66-COOCu and UiO-66-$(COOCu)_2$, respectively. NH_3 dynamic capacities for all materials are presented in Table 11.

Under dry and wet conditions, UiO-66-$(COOCu)_2$ shows an ammonia dynamic capacity of 6.38 mmol g^{-1} and 6.84 mmol g^{-1} (higher than UiO-66-COOCu in both cases), even though it has a lower surface area and copper loading. This infers that there is not a direct correlation between metal loading and ammonia uptake, probably due to pore blocking caused by the introduction of metal ions. In the case of UiO-66-COOCu it is probable that copper ions coordinate to carboxylic acid groups not only on the surface but on the inside of the framework as well, hindering the access of NH_3 molecules to the adsorption sites. In contrast, given the higher number of –COOH groups in UiO-66-$(COOH)_2$ it is unlikely for copper ions to access the –COOH sites inside the framework. Therefore, it is most likely that copper coordinates to only the carboxylate groups pointing outwards from the MOF surface where is more accessible for NH_3 molecules to adsorb.

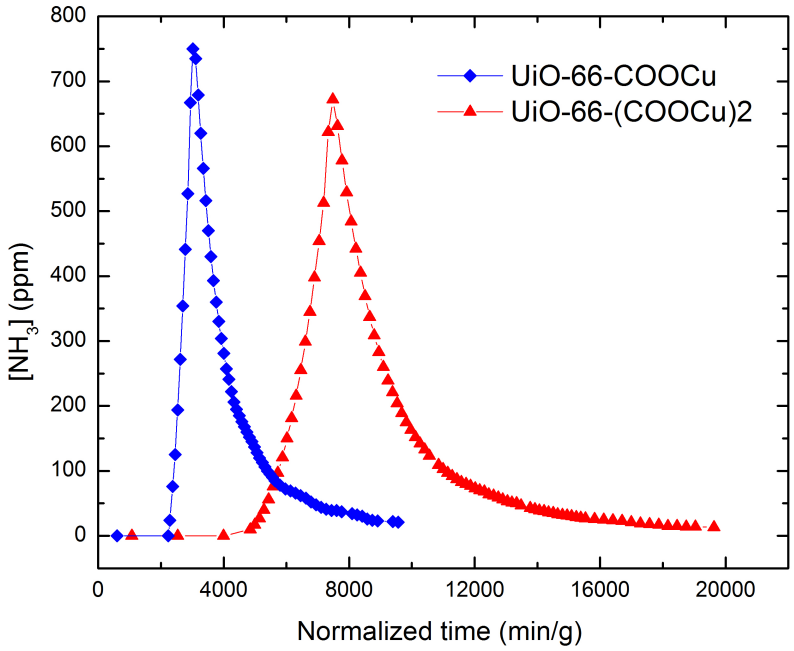

Figure 17. Dry ammonia breakthrough curves for UiO-66-COOCu and UiO-66-$(COOCu)_2$.

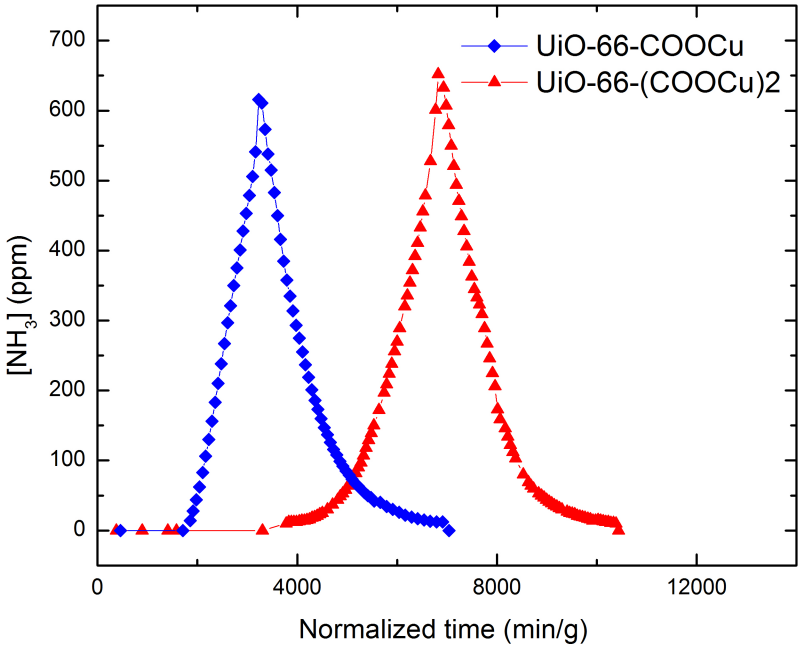

Figure 18. Wet ammonia breakthrough curves for UiO-66-COOCu and UiO-66-$(COOCu)_2$.

Table 11. Dry and wet ammonia dynamic capacities of MOFs included in this study.

MOF	NH_3 Dynamic Capacity (mmol g^{-1})	
	Dry (0% RH)	Wet (80% RH)
UiO-66-COOH_S2	2.24	2.21
UiO-66-COOCu	3.04	3.10
[a]UiO-66-$(COOH)_2$	2.83	1.83
UiO-66-$(COOCu)_2$	6.38	6.84

[a]Data from Jasuja, et al.[26]

Both metalated MOFs exhibit almost no change in NH_3 capacity under humid conditions which differs from the behavior of other UiO-66 versions.[26] Less steep slopes found for wet conditions are an indication of higher mass transfer limitations caused by the presence of water molecules during NH_3 adsorption, but no capacity drop was observed for either of these MOFs. Moreover, Snurr and coworkers[25] demonstrated that –COOCu groups have a stronger preference for NH_3 over water, when compared to –COOH groups.

Comparison between NH_3 dynamic capacities for metalated and non-metalated samples (Table 12) shows that the dry NH_3 capacities increased by 36% and 125% for UiO-66-COOCu and UiO-66-$(COOCu)_2$. This is consistent with results reported from computational studies,[25] which show that the binding energy of NH_3 is higher with –COOCu than with –COOH functional groups (approximately 4 times higher).

The fact that the curves don't show any unusual shapes or additional steps (Figure 18) infer that the materials are not decomposing after NH_3 exposure under humid

conditions, like in the case of other adsorbents such as DMOF-TM2 and ZnBTTB.[26] To test this, PXRD and N_2 phisysorption data (Figure 19) were collected for the samples before and after ammonia exposure under humid conditions. As shown in Table 12, there is a slight loss in surface area for both materials, suggesting that both materials are partially stable after humid NH_3 exposure. This loss in surface area is puzzling compared to the results obtained from water vapor adsorption experiments where neither the materials exhibited a loss in surface area. Humid NH_3 exposed samples were regenerated before N_2 physisorption analysis. It is still unclear whether this apparent loss in surface area is caused by NH_3 exposure alone or by the humid conditions to which the samples were exposed. In the future, N_2 physisorption analysis should be conducted for the samples after NH_3 exposure under dry conditions.

PXRD patterns of the metalated samples before and after exposure to humid NH_3 vapor were also collected. As can be seen in Figure 20, no apparent loss in crystallinity is observed for the samples after humid NH_3 exposure, suggesting the materials are not decomposing along the wet breakthrough experiments.

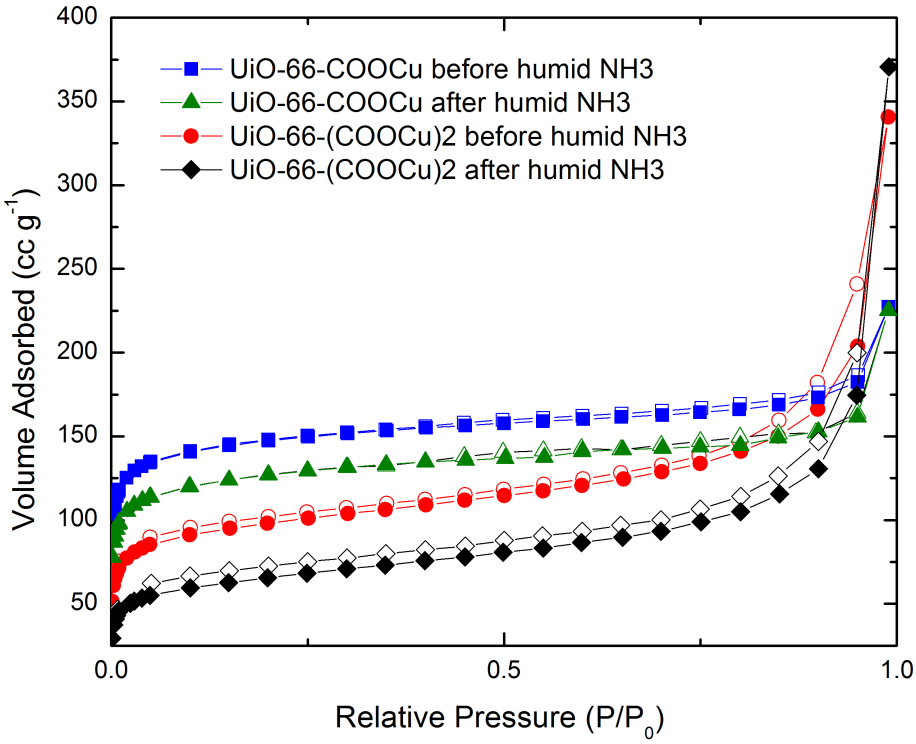

Figure 19. Nitrogen adsorption for samples before and after humid ammonia breakthrough experiments. (closed symbols - adsorption, open symbols – desorption).

Table 12. BET surface area analysis before and after humid ammonia exposure.

MOF	BET Surface Area (m^2 g^{-1})		
	Before	After	% Loss
UiO-66-COOCu	564	447	15
UiO-66-$(COOCu)_2$	357	229	36

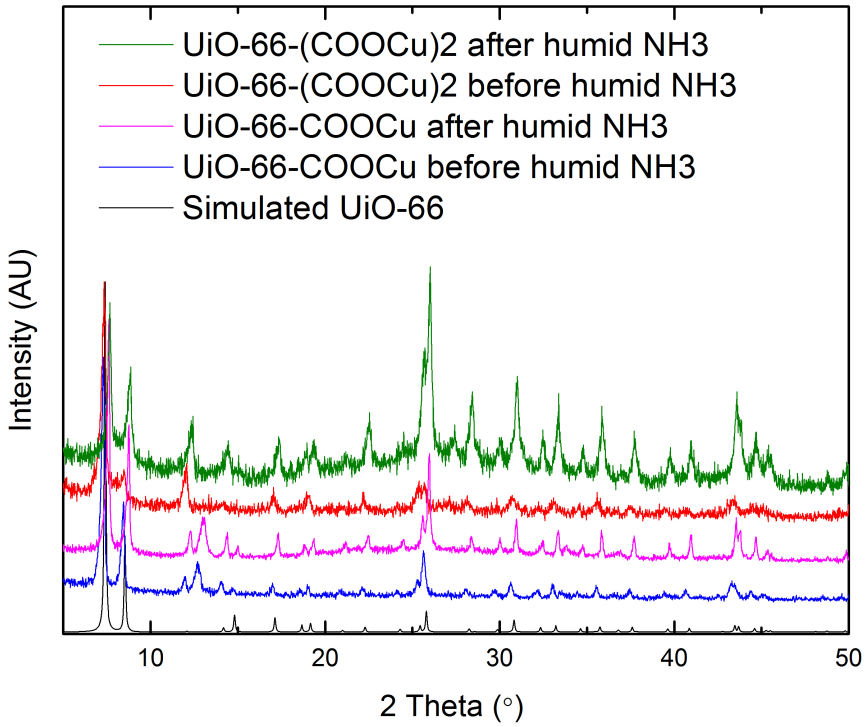

Figure 20. Comparison between PXRD patterns of samples before and after humid ammonia breakthrough experiments, and theoretical pattern of UiO-66.

CHAPTER 4

CONCLUSIONS AND RECOMMENDATIONS FOR FUTURE WORK

4.1 Conclusions

UiO-66 versions functionalized with copper carboxylate groups were identified as potential candidates for ammonia removal from air. Zr-BDC MOFs with –COOCu and $–(COOCu)_2$ groups were synthesized in this study by a post synthetic modification of the UiO-66-COOH and UiO-66-$(COOH)_2$ frameworks, respectively. Metal insertion was conducted in the presence of DMF at 65°C for 24 h. From the different parameters tested in this study, these conditions resulted in the highest copper loadings given the observed mass transfer (pore space, solvent size) and kinetic (time, temperature) limitations. Still, low copper loadings were obtained and attributed to the restricted pore spaces in UiO-66-COOH and UiO-66-$(COOH)_2$.

Copper carboxylate functionalized versions of UiO-66 were found to have higher ammonia capacities than other UiO-66 functionalities under, both, dry and humid conditions. This increase in NH_3 loadings is due to the higher binding energy of NH_3 with the copper carboxylate groups when compared to carboxylic acid groups, as demonstrated by computational studies.[25] Materials exhibit no loss in capacity under humid conditions in contrast with other UiO-66 functionalities.[26] Among the MOFs studied, the material with $–(COOCu)_2$ groups had a higher NH_3 loading than UiO-66-COOCu although it had a lower copper loading. This result is probably due to the fact that because of its lower pore space, most of the coordinated copper ions are in the outer surface of the framework where it is easier for NH_3 molecules to adsorb. Table 13

summarizes the textural properties of the metalated samples, as well as the results obtained from dry and wet ammonia breakthrough experiments. Although no direct correlation between ammonia dynamic capacities and copper loading or surface area can be derived, results show that the ammonia uptake increases after metal complexation with the uncoordinated carboxylic acid groups of UiO-66-COOH and UiO-66-$(COOH)_2$.

Table 13. Properties and ammonia dynamic capacities of MOFs included in this work.

MOF	Copper Loading (Cu/Zr Mass Ratio)	[a]Surface Area (m^2 g^{-1})	NH_3 Dynamic Capacity (mmol g^{-1})	
			Dry (0% RH)	Wet (80% RH)
UiO-66-COOH	0	658	2.24	2.21
UiO-66-COOCu	0.38	564	3.04	3.10
[b]UiO-66-$(COOH)_2$	0	364	2.83	1.83
UiO-66-$(COOCu)_2$	0.12	357	6.38	6.84

[b]BET Analysis.
[b]Data from Jasuja, et al.[26]

Results from this study lead us to conclude that UiO-66-$(COOCu)_2$ has a high potential for air purification applications; specially for ammonia adsorption. To the best of our knowledge, copper carboxylate groups are among the functional groups of UiO-66 with the highest performance towards ammonia removal from air.

4.2 Recommendations for Future Work

4.2.1 More Extensive Characterization of Metalated Samples

Although XPS provides a method to determine the copper oxidation state after metal complexation, a more extensive characterization of the metalated samples should be conducted. Additional techniques should be employed in order to further elucidate the coordination nature of copper ions into the UiO-66-COOH and UiO-66-$(COOH)_2$ frameworks. Several techniques can be used to probe the copper environment on metalated samples, such as Electron paramagnetic resonance (EPR)[48] and Extended X-ray adsorption fine structure (EXAFS).[50] Density functional theory (DFT) calculations can also be used to determine the MOFs adsorption sites available for copper complexation.[40]

4.2.2 Incorporate Metal Carboxylate Groups into MOFs with Bigger Pore Spaces

Even though successful grafting of copper atoms into the –COOH functional groups of UiO-66-COOH and UiO-66-$(COOH)_2$ was attained in this work, the copper loading on these materials is highly restricted by the pore space available for metal complexation. Other water-stable MOFs with larger pore space, such as the MIL-101 series, should be investigated as candidates for functionalization with metal carboxylate groups. Recently, Hartmann, et al.[58] and Serra-Crespo, et al.[59] successfully reported the synthesis of amino functionalized version of MIL-101(Al). Similar synthesis methods should be investigated to synthesize MIL-101(Al) with –COOH and –$(COOH)_2$ functional groups and subsequent modification to incorporate –COOCu groups into the

frameworks. Moreover, the incorporation of metal (Cu, Pt) nanoparticles into such frameworks has also been proven to be effective in catalysis applications.[60,61]

In addition, it has been shown that ammonia loading on porous materials is highly limited by the pore space available for ammonia adsorption. As previously mentioned, a blocked pore space restricts the entry of ammonia molecules onto the pores of the materials and its access to available adsorption sites. MOFs with bigger pore spaces than UiO-66 should have more available pore space even after metal complexation. Materials with various copper loadings should be synthesized and tested for ammonia adsorption to investigate the effect of pore blocking (caused by the incorporation of metals into the frameworks) on ammonia uptake.

4.2.3 Investigate the Effect of Water Addition on the Synthesis of UiO-66-COOH

As previously explained in Chapter 2, the addition of water to the synthesis of UiO-66-COOH (and other UiO-66 versions in our lab) has proven to increase the quality and synthesis yield (to some extent) of the final product. Although effective, the reason for this is still unknown. Peterson et al.[62] reported the addition of water to a Zirconium (IV) chloride-DMF mixture prior to the addition of the 2-Aminoterephthalic acid ligand (in DMF) in the synthesis of UiO-66-NH_2. The UiO-66-NH_2 synthesis, in this case, was modified from previous methods to render a large scale synthesis, but the effect of the water addition on the synthesis properties was not explained. Work done by Schaate, et al.[63] also found water to be essential on the synthesis of well-ordered Zr-bdc-NH_2. Other studies have analyzed the influence of different modulators,[42,63-64] such as benzoic acid, acetic acid, HCl and formic acid on the synthesis of Zr-based MOFs; but a complete study on the effect of water addition to the synthesis procedures is still lacking. In the

future, a detailed study on the effect of water inclusion on the synthesis of functionalized UiO-66 versions should be conducted. Properties such as crystal and particle size, morphology and porosity should be investigated after the addition of water to the synthesis methods.

4.2.4 Identify Other Experimental Methods to Increase Copper Loading

This work provided the first step in the incorporation and characterization of copper carboxylate groups (-COOCu) into the UiO-66 frameworks functionalized with uncoordinated carboxylic acid groups. While the inclusion of copper ions was successful in UiO-66-COOH and UiO-66-$(COOH)_2$, the copper loadings obtained for both materials was substantially low compared to theoretical values. Other techniques should be investigated with the aim of increasing the metal uptake by these materials. Experimental methods that allow for mass transfer and kinetic limitations to be minimized, such as sonication, longer reaction times and other solvents should be employed on the study of metal insertion on these and other MOFs.

APPENDIX A

AMMONIA ADSORPTION ON UiO-66-COOH

In order to determine the increase in ammonia adsorption capacity, after metal insertion, of UiO-66-COOCu, ammonia breakthrough studies were conducted under dry and humid conditions with UiO-66-COOH. The samples were activated at 65°C for 2 h in-situ prior to the breakthrough runs. Experimental procedure and set up is as previously described in Section 2.4. Figure 21 shows the breakthrough curves for wet and dry conditions. The low steepness of the curve under wet conditions implies higher mass transfer limitations.

Although, this MOF was not characterized after the breakthrough studies, the fact that there are not unusual steps or shape of the curve infer that the framework is not decomposing under humid conditions. A drop in ammonia dynamic capacity occurs for wet studies, similar to other UiO-66 functionalities,[26] probably due to the competition between water and ammonia for the adsorption sites. As observed in Table 14, UiO-66-COOH has a lower ammonia capacity than UiO-66-$(COOH)_2$ due to a lower concentration of active sites. Ammonia loading under dry conditions of UiO-66-COOH is of the same magnitude as the value (2.24 mmol g^{-1}) reported by DeCoste et al.[65] for a UiO-66 analogue with uncoordinated –COOH groups. This slightly higher value may be due to the fact, that although for this analogue there are less carboxylic acid groups (and therefore, adsorption sites), there is more pore space available for the entry of ammonia molecules into the framework, due to defects in the material purposely created.

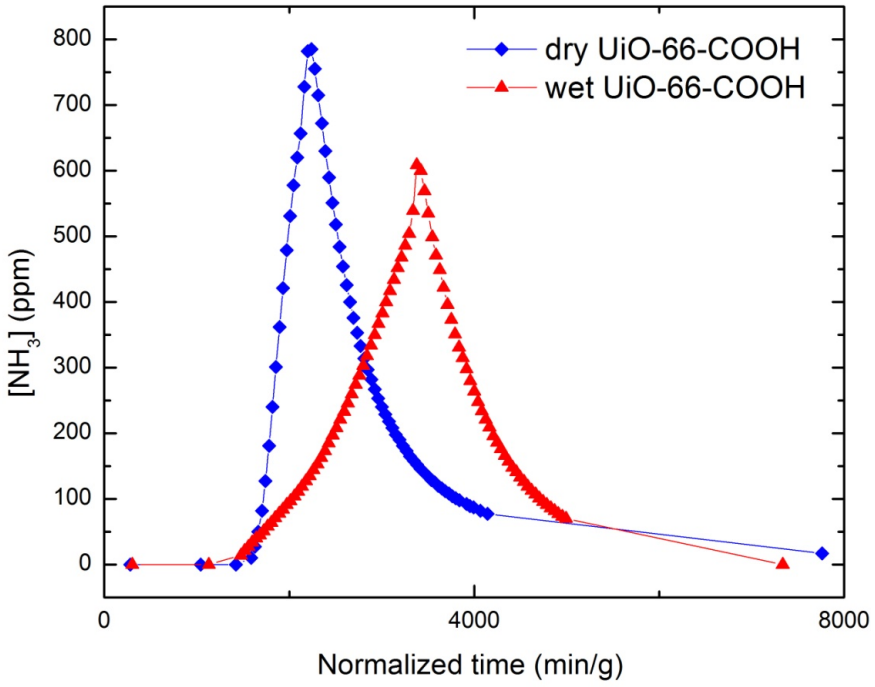

Figure 21. Ammonia breakthrough curves for dry and wet conditions for UiO-66-COOH.

Table 14. Comparison between ammonia dynamic capacities of UiO-66-COOH and UiO-66-$(COOH)_2$.

MOF	NH_3 Dynamic Capacity (mmol g^{-1})	
	Dry (0% RH)	Wet (80% RH)
UiO-66-COOH_S2	2.24	2.21
[a]UiO-66-$(COOH)_2$	2.83	1.83

APPENDIX B

RAW DATA

B.1 Water Vapor Gas Adsorption/Desorption

Table 15. Water vapor adsorption isotherm data for UiO-66-COOCu at 298 K.

Adsorption		Desorption	
RH (%)	Loading (mmol g-1)	RH (%)	Loading (mmol g-1)
0.0000	0.0000	89.3490	14.5998
10.6920	3.7787	79.4880	14.0113
20.5260	7.2086	59.8520	13.2763
30.3690	9.9710	40.1910	12.4750
40.1890	11.2203	20.5390	9.3793
50.0180	12.2777	0.0000	1.4569
59.8540	12.8758		
69.6900	13.2421		
79.4960	13.7754		
89.3490	14.5998		

Table 16. Water vapor adsorption isotherm data for UiO-66-$(COOCu)_2$ at 298 K.

Adsorption		Desorption	
RH (%)	Loading (mmol g-1)	RH (%)	Loading (mmol g-1)
0.0000	0.0000	89.3360	16.1833
10.6900	7.0937	79.5010	14.8128
20.5390	9.1814	59.8550	12.4451
30.3610	10.1562	40.1870	11.3059
40.1920	10.8908	20.5350	9.9632
50.0220	11.5439	0.0000	1.0964
59.8550	12.4848		
69.6750	13.0963		
79.5070	14.3088		
89.3360	16.1833		

B.2 Ammonia Breakthrough Experiments

All data from repeatability studies is available at S:\Research\Walton group\MEMBERS FOLDERS\Erika\Ammonia Breakthrough.

Table 17. Dry ammonia breakthrough raw data for UiO-66-COOH.

Mass activated material: 0.0131g

Adsorption		Desorption	
Normalized time (min g^{-1})	$[NH_3]$ (ppm)	Normalized time (min g^{-1})	$[NH_3]$ (ppm)
0	0	2276	755
1590	10	2314	715
1628	27	2353	672
1666	50	2391	630
1704	82	2429	590
1742	127	2467	551
1781	181	2505	518
1819	240	2543	484
1857	301	2581	454
1895	362	2619	426
1933	421	2658	400
1971	479	2696	376
2009	531	2734	353
2047	578	2772	333
2086	620	2810	314
2124	657	2848	297
2162	728	2886	282
2200	782	2924	267
2238	785	2963	253
		3001	240
		3039	229
		3077	218
		3115	208
		3153	198

Table 17 (continued).

Adsorption		Desorption	
Normalized time (min g^{-1})	[NH_3] (ppm)	Normalized time (min g^{-1})	[NH_3] (ppm)
		3191	190
		3229	181
		3268	173
		3306	165
		3344	158
		3382	152
		3420	146
		3458	140
		3496	135
		3534	129
		3573	125
		3611	120
		3649	116
		3687	112
		3725	108
		3763	104
		3801	101
		3839	98
		3916	92
		3954	89
		3992	87
		4068	82
		4144	77
		7760	17

Table 18. Wet ammonia breakthrough raw data for UiO-66-COOH.

Mass activated material: 0.0121g

Adsorption		Desorption	
Normalized time (min g^{-1})	$[NH_3]$ (ppm)	Normalized time (min g^{-1})	$[NH_3]$ (ppm)
0	0	3421	600
1477	14	3462	569
1518	21	3504	535
1560	27	3545	499
1601	34	3587	471
1642	40	3628	449
1684	45	3669	422
1725	51	3711	396
1766	58	3752	373
1808	64	3793	351
1849	71	3835	331
1891	78	3876	315
1932	84	3917	298
1973	91	3959	280
2015	97	4000	264
2056	104	4042	248
2097	111	4083	234
2139	119	4124	221
2180	127	4166	209
2221	135	4207	196
2263	144	4248	186
2304	153	4290	176
2346	163	4331	166
2387	173	4373	157
2428	185	4414	148
2470	197	4455	141
2511	208	4497	133
2552	221	4538	126

Table 18 (continued).

Adsorption		Desorption	
Normalized time ($min\ g^{-1}$)	$[NH_3]$ (ppm)	Normalized time ($min\ g^{-1}$)	$[NH_3]$ (ppm)
2594	233	4579	119
2635	246	4621	113
2676	260	4662	107
2718	274	4703	101
2759	288	4745	96
2801	303	4786	91
2842	318	4828	86
2883	334	4869	82
2925	350	4910	77
2966	367	4952	73
3007	383	4993	70
3049	400	7336	0
3090	417		
3132	434		
3173	452		
3214	468		
3256	486		
3297	504		
3338	539		
3380	609		

Table 19. Dry ammonia breakthrough raw data for UiO-66-COOCu.

Mass of activated material: 0.00612g

Adsorption		Desorption	
Normalized time (min g^{-1})	$[NH_3]$ (ppm)	Normalized time (min g^{-1})	$[NH_3]$ (ppm)
0	0	3105	735
2288	24	3186	679
2369	76	3268	620
2451	125	3350	566
2533	194	3431	516
2614	272	3513	470
2696	354	3595	430
2778	441	3677	393
2860	527	3758	360
2941	667	3840	330
3023	750	3922	304
		4003	281
		4085	257
		4167	241
		4248	222
		4330	206
		4412	195
		4494	185
		4575	176
		4657	168
		4739	160
		4820	152
		4902	145
		4984	137
		5065	128
		5147	120
		5229	113
		5311	106

Table 19 (continued).

Adsorption		Desorption	
Normalized time (min g^{-1})	[NH_3] (ppm)	Normalized time (min g^{-1})	[NH_3] (ppm)
		5392	100
		5474	95
		5555.56	90
		5637	85
		5801	78
		5964	72
		6128	69
		6291	66
		6454	62
		6618	58
		6781	52
		6944	48
		7108	44
		7271	41
		7435	39
		7598	39
		7761	37
		8088	34
		8252	32
		8415	30
		8578	26
		8742	24
		8905	23
		9395	22
		9559	21

Table 20. Wet ammonia breakthrough raw data for UiO-66-COOCu.

Mass of activated material: 0.0080g

Adsorption		Desorption	
Normalized time (min g^{-1})	[NH_3] (ppm)	Normalized time (min g^{-1})	[NH_3] (ppm)
0	0	3291	611
1855	14	3353	573
1917	28	3416	538
1980	44	3478	515
2042	62	3541	483
2104	83	3603	450
2167	106	3666	416
2229	130	3728	385
2292	156	3790	358
2354	183	3853	335
2417	210	3915	314
2479	238	3978	293
2542	267	4040	275
2604	297	4103	255
2666	321	4165	237
2729	350	4228	219
2791	375	4290	201
2854	401	4352	186
2916	428	4415	173
2979	453	4477	160
3041	479	4540	147
3104	506	4602	137
3166	541	4665	126
3228	616	4727	116
		4790	108
		4852	99
		4915	92
		4977	85

Table 20 (continued).

Adsorption		Desorption	
Normalized time (min g^{-1})	[NH_3] (ppm)	Normalized time (min g^{-1})	[NH_3] (ppm)
		5039	79
		5102	73
		5164	67
		5227	63
		5289	58
		5352	54
		5414	50
		5477	47
		5539	42
		5664	40
		5789	34
		5914	30
		6039	26
		6163	22
		6288	19
		6413	17
		6538	15
		6663	13
		6788	12
		6913	12
		7038	0

Table 21. Dry ammonia breakthrough raw data for UiO-66-$(COOCu)_2$.

Mass of activated material: 0.0034g

Adsorption		Desorption	
Normalized time (min g^{-1})	$[NH_3]$ (ppm)	Normalized time (min g^{-1})	$[NH_3]$ (ppm)
0	0	7629	631
4848	10	7775	578
4995	17	7921	529
5141	27	8068	484
5287	40	8214	442
5434	56	8360	405
5580	76	8507	369
5726	97	8653	337
5873	121	8799	309
6019	150	8946	283
6165	181	9092	260
6312	216	9238	239
6458	255	9385	221
6604	299	9531	204
6751	345	9677	189
6897	398	9823	175
7043	454	9970	163
7190	513	10116	152
7336	622	10262	142
7482	672	10409	133
		10555	123
		10848	109
		10994	103
		11140	97
		11287	92
		11433	87
		11579	83
		11726	80

Table 21 (continued).

Adsorption		Desorption	
Normalized time (min g^{-1})	[NH_3] (ppm)	Normalized time (min g^{-1})	[NH_3] (ppm)
		11872	77
		12018	73
		12165	70
		12311	68
		12457	64
		12604	62
		12750	59
		12896	56
		13043	53
		13189	51
		13335	50
		13482	47
		13774	43
		13921	41
		14067	39
		14213	38
		14360	36
		14506	35
		14652	33
		14799	32
		14945	31
		15091	30
		15238	29
		15384	28
		15530	27
		15823	26
		16116	25
		16408	24
		16701	23

Table 21 (continued).

Adsorption		Desorption	
Normalized time (min g^{-1})	[NH_3] (ppm)	Normalized time (min g^{-1})	[NH_3] (ppm)
		16994	21
		17286	19
		17579	18
		17871	17
		18164	15
		18457	15
		18749	14
		19042	14
		19627	13

Table 22. Wet ammonia breakthrough raw data for UiO-66-$(COOCu)_2$.

Mass of activated material: 0.0097g

Adsorption		Desorption	
Normalized time ($min\ g^{-1}$)	$[NH_3]$ (ppm)	Normalized time ($min\ g^{-1}$)	$[NH_3]$ (ppm)
3781	10	6928	633
3832	12	6980	607
3884	12	7031	579
3935	12	7083	550
3987	12	7135	521
4039	13	7186	494
4090	14	7238	471
4142	14	7289	449
4193	15	7341	428
4245	16	7393	406
4297	18	7444	384
4348	19	7496	363
4400	21	7547	345
4451	23	7599	333
4503	25	7651	323
4606	30	7702	309
4709	37	7754	289
4813	44	7805	267
4864	49	7857	246
4916	53	7909	225
4967	58	7960	206
5019	64	8012	173
5071	69	8063	159
5174	82	8167	146
5225	90	8218	134
5277	97	8270	122
5329	107	8321	112
5380	118	8373	103

Table 22 (continued).

Adsorption		Desorption	
Normalized time (min g^{-1})	$[NH_3]$ (ppm)	Normalized time (min g^{-1})	$[NH_3]$ (ppm)
5432	129	8528	80
5483	139	8631	69
5535	150	8683	64
5638	172	8734	60
5741	197	8837	53
5793	209	8889	50
5845	224	8941	47
5896	238	8992	44
5948	256	9044	41
5999	270	9095	39
6051	289	9147	36
6154	320	9199	34
6206	336	9250	32
6257	354	9302	30
6309	372	9405	27
6361	392	9457	25
6412	411	9508	24
6464	433	9560	23
6515	456	9611	21
6567	479	9663	20
6670	528	9715	19
6773	601	9766	18
6825	652	9818	17
		9869	16
		9921	14
		9973	14
		10024	15
		10076	14
		10127	13

Table 22 (continued.)

Adsorption		Desorption	
Normalized time (min g^{-1})	$[NH_3]$ (ppm)	Normalized time (min g^{-1})	$[NH_3]$ (ppm)
		10179	12
		10231	12
		10282	11
		10334	11
		10385	10
		10437	0

REFERENCES

1. Yaghi, O. M.; O'Keeffe, M.; Ockwig, N.W.; Chae, H. K.; Eddaoudi, M.; Kim, J. Reticular synthesis and the design of new materials. *Nature* **2003**, *423*, 705-713.

2. Férey, G. Hybrid porous solids: past, present, future. *Chem. Soc. Rev.* **2008**, *37*, 191-214.

3. Furukawa, H.; Cordova, K.E.; O'Keeffe, M.; Yaghi, O. M. The Chemistry and Applications of Metal-Organic Frameworks. *Science* **2013**, *341*.

4. Furukawa, H.; Ko, N.; Go, Y. B.; Aratani, N.; Choi, S. B.; Choi, E.; Yazaydin, A. O.; Snurr, R.; O'Keeffe, M.; Kim, J.; Yaghi, O. M. Ultrahigh Porosity in Metal-Organic Frameworks. *Science* **2010**, *329*, 424-428.

5. Farha, O. K.; Eryazici, L.; Jeong, N. C.; Hauser, B. G.; Wilmer, C. E.; Sarjeant, A.A; Snurr, R. Q.; Nguyen, S. T.; Yazaydin, A. Ö.; Hupp, J. T. Metal-Organic Framework Materials with Ultrahigh Surface Areas: Is the Sky the Limit? *J. Am. Chem. Soc.* **2012**, *134*, 15016-15021.

6. Murray, L.J.; Dinca, M.; Long, J.R. Hydrogen storage in metal-organic frameworks. *Chem. Soc. Rev.* **2009**, *38*, 1294-1314.

7. Getman, R. B.; Bae, Y.-S.; Wilmer, C. E.; Snurr, R. Q. Review of Molecular Simulations of Methane, Hydrogen, and Acetylene Storage in Metal-Organic Frameworks. *Chem. Rev.* **2012**, *112*, 703-723.

8. Li, J. R.; Kuppler, R. J.; Zhou, H.-C. Selective gas adsorption and separation in metal-organic frameworks. *Chem. Soc. Rev.* **2009**, *38*, 1477-1504.

9. Li, J.-R.; Sculley, J.; Zhou, H.-C. Metal-Organic Frameworks for Separations. *Chem. Rev.* **2012**, *112*, 869-932.

10. Lee, J.; Farha, O.K.; Roberts, J.; Scheidt, K. A.; Nguyen, S. T.; Hupp, J. T. Metal-organic framework materials as catalysts. *Chem. Soc. Rev.* **2009**, *38*, 1450-1459.

11. Khan, N. A.; Hasan, Z.; Jhung, S. H. Adsorptive removal of hazardous materials using metal-organic frameworks (MOFs): A review. *J. Hazard. Mater.* **2013**, *244-245*, 444-456.

12. DeCoste, J.B.; Peterson, G.W. Metal-Organic Frameworks for Air Purification of Toxic Chemicals. *Chem. Rev.* **2014**, *114*, 5695-5727.

13. Keskin, S.; Kizilel, S. Biomedical Applications of Metal Organic Frameworks. *Ind. Eng. Chem. Res.* **2011**, *50*, 1799-1812.

14. Kreno, L. E.; Leong, K.; Farha, O. K.; Allendorf, M.; Van Duyne, R. P.; Hupp, J. T. Metal-Organic Framework Materials as Chemical Sensors. *Chem. Rev.* **2012**, *112*, 1105-1125.

15. Eddaoudi, M.; Kim, J.; Rosi, N.; Vodak, D.; Wachter, J.; O'Keeffe, M.; Yaghi, O. M. Systematic Design of Pore Size and Functionality in Isoreticular MOFs and Their Application in Methane Strage. *Science* **2002**, *295*, 469-472.

16. Wang, Z.; Cogen, S. M. Postsynthetic modification of metal-organic frameworks. *Chem. Soc. Rev.* **2009**, *38*, 1315-1329.

17. Britt, D.; Tranchemontagne, D.; Yaghi, O. M. Metal-organic frameworks with high capacity and selectivity for harmful gases. *Proc. Natl. Acad. Sci. U.S.A.* **2008**, *105* (33), 11623-11627.

18. Jacoby, M. Air Filters for the Face. *Science and Technology*. CEN.ACS.ORG **2014**.

19. Morrison, R.W. NBC Filter Performance, Edgewood Chemical Biological Center, 2001.

20. Karwacki, C. J.; Jones, P. Toxic Industrial Chemicals Assessment of NBC Filter Performance, Edgewood Chemical Biological Center, 2000.

21. The Facts About Ammonia. Department of Health, NY, U. S. https://www.health.ny.gov/environmental/emergency/chemical_terrorism/ammonia_tech.htm, last accessed on 03/31/2015.

22. Toxicological Profile for Ammonia. U. S. Department of Health and Human Services. Agency for Toxic Substances and Disease Registry. 2002. http://www.atsdr.cdc.gov/toxprofiles/tp126.pdf, last accessed on 03/31/2015.

23. Hincal, F.; Erkekoglu, P. FABAD J. Pharm. Sci., 31, 220-229, 2006

24. Karasik, T. Toxic Warfare. RAND: Santa Monica, CA, 2002.

25. Kim, K. C.; Yu, D.; Snurr, R. Q. Computational Screening of Functional Groups for Ammonia Capture in Metal-Organic Frameworks. *Langmuir* **2013**, *29*, 1446-1456.

26. Jasuja, H.; Peterson, G. W.; DeCoste, J. B.; Browe, M. A.; Walton, K. S. Evaluation of MOFs for air purification and air quality control applications: Ammonia removal from air. *Chem. Eng. Sci.* **2015**, *124*, 118-124.

27. Spanopoulos, I.; Xydias, P.; Malliakas, C. D.; Trikalitis, P. A Straight Forward Route for the Development of Metal-Organic Frameworks Functionalized with Aromatic –OH Groups: Synthesis, Characterization, and Gas (N2, Ar, H2, CO2, CH4, NH3) Sorption Properties. *Inorg. Chem.* **2013**, *52*, 855-862.

28. Morris, W.; Doonan, C. J.; Yaghi, O. M. Postsynthetic Modification of a Metal-Organic Framework for Stabilization of a Hemiaminal and Ammonia Uptake. *Inorg. Chem.* **2011**, *50*, 6853-6855.

29. DeCoste, J. B.; Demasky, T. J.; Katz, M. J.; Farha, O. K.; Hupp, J. T. A UiO-66 analogue with uncoordinated carboxylic acids for the broad-spectrum removal of toxic chemicals. *New J. Chem.* **2015**, (DOI: 10.1039/C4NJ02093F).

30. Mu, B.: Synthesis and gas adsorption study of porous metal-organic framework materials, Ph.D. Thesis, Georgia Institute of Technology, Atlanta, GA, 2011.

31. Barea, E.; Montoro, C.; Navarro J. A. R. Toxic gas removal – metal-organic frameworks for the capture and degradation of toxic gases and vapours. *Chem. Soc. Rev.* **2014**, *43*, 5419.

32. Peterson, G. W.; Wagner, G. W.; Balboa, A.; Mahle, J.; Sewell, T.; Karwacki, C. J. Ammonia Vapor Removal by Cu3(BTC)2 and its Characterization by MAS NMR. *J. Phys. Chem. C* **2009**, *113*, 13906-13917.

33. Glover, T. G.; Peterson, G. W.; Schindler, B. J.; Britt, D.; Yaghi, O. MOF-74 building unit has a direct impact on toxic gas adsorption. *Chem. Eng. Sci.* **2011**, *66*, 163-170.

34. Cavka, J. H.; Jakobsen, S.; Olsbye, U.; Guillou, N.; Lamberti, C.; Bordiga, S.; Lillerud, K. P. A New Zirconium Inorganic Building Brick Forming Metal-Organic Frameworks with Exceptional Stability. *J. Am. Chem. Soc.* **2008**, *130*, 13850-13851.

35. Cmarik, G. E.; Kim, M.; Cohen, S. M.; Walton, K. S. Tuning the Adsorption Properties of UiO-66 via Ligand Functionalization. *Langmuir* **2012**, *28*, 15606-15613.

36. Schoenecker, P. M.; Carson, C. G.; Jasuja, H.; Flemming, C. J. J.; Walton, K. S. Effect of Water Adsorption on Retention of Structure and Surface Area of Metal-Organic Frameworks. *Ind. Eng. Chem. Res.* **2012**, *51*, 6513-6519.

37. Jasuja, H.; Zang, J.; Sholl, D. S.; Walton, K. S. Rational Tuning of Water Vapor and CO2 Adsorption in Highly Stable Zr-Based MOFs. *J. Phys. Chem. C* **2012**, *116*, 23526-23532.

38. Yu, D.; Ghosh, P.; Snurr, R. Q. Hierarchical modeling of ammonia adsorption in functionalized metal-organic frameworks. *Dalton Trans.* **2012**, *41*, 3962.

39. Gadzikwa, T.; Farha, O. K.; Mulfort, K. L.; Hupp, J. T.; Nguyen, S. T. A Zn-based, pillared paddlewheel MOF containing free carboxylic acids via covalent post-synthesis elaboration. *Chem. Commun.* **2009**, 3720-3722.

40. Meng, X.; Zhong, R.; Song, X.; Song, S.; Hao, Z.; Zhu, M.; Zhao, S.; Zhang, H. A stable, pillar-layer metal-organic framework containing uncoordinated carboxyl groups for separation of transition metal ions. *Chem. Commun.* **2014**, *50*, 6406.

41. Lee, Y.; Kim, S.; Kang, J. K.; Cohen, S. M. Photocatalytic CO2 reduction by a mixed metal (Zr/Ti), mixed ligand metal-organic framework under visible light irradiation. *Chem. Commun*. **2015**, *51*, 5735.

42. Biswas, S.; Van Der Voort, P. A General Strategy for the Synthesis of Functionalized UiO-66 Frameworks: Characterization, Stability and CO2 Adsorption Properties. *Eur. J. Inorg. Chem.* **2013**, 2154–2160.

43. Biswas, S.; Zhang, J.; Li, Z.; Liu, Y.–Y.; Grzywa, M.; Sun, L.; Volkmer, D.; Van Der Voort, P. Enhanced selectivity of CO2 over CH4 in sulphonate-, carboxylate- and iodo-functionalized UiO-66 frameworks. *Dalton Trans*. **2013**, *42*, 4730.

44. Walton, K. S.; Snurr, R. Q. Applicability of the BET Method for Determining Surface Areas of Microporous Metal-Organic Frameworks. *J. AM. CHEM. SOC.* **2007**, *129*, 8552-8556.

45. Yang, Q.; Wiersum, A. D.; Llewellyn, P. L.; Guillerm, V.; Serre, C.; Maurin, G. Functionalizing porous zirconium terephthalate UiO-66(Zr) for natural gas upgrading: a computational exploration. *Chem. Commun.* **2011**, *47*, 9603-9605.

46. Lau, C. H.; Babarao, R.; Hill, M. R. A route to drastic increase of CO2 uptake iin Zr metal organic framework UiO-66. *Chem. Commun.* **2013**, *49*, 3634.

47. Elshof, J. E.; Abadal, C. R.; Sekulić, J.; Chowdhury, S. R.; Blank, D. H.A. Transport mechanisms of water and organic solvents through microporous silica in the pervaporation of binary liquids. *Micro. and Meso. Mater.* **2003**, *65*, 197-208.

48. Valvekens, P.; Bloch, E. D.; Long, J. R.; Ameloot, R.; De Vos D. E. Counteranion effects on the catalytic activity of copper salts immobilized on the 2,2'-bipyridine-functionalized metal-organic framework MOF-253. *Catalysis Today*. **2015**, *246*, 55-59.

49. Andreu, C.; Sanz, F.; Asensio, G. Counterion's Effect on the Catalytic Activity of Zn-Prolinamide Complexes in Aldol Condensations. *Eur. J. Org. Chem.* **2012**, 4185-4191.

50. Bloch, E. D.; Britt, D.; Lee, C.; Doonan, C. J.; Uribe-Romo, F. J.; Furukawa, H.; Long, J. R.; Yaghi, O. M. Metal Insertion in a Microporous Metal-Organic Framework Lined with 2,2'-Bipyridine. *J. Am. Chem. Soc.* **2010**, *132*, 14382-14384.

51. Jasuja, H.: Developing Design Criteria and Scale-up Methods for Water-Stable Metal-Organic Frameworks for Adsorption Applications, Ph.D. Thesis, Georgia Institute of Technology, Atlanta, GA, 2014.

52. Kandiah, M.; Nilsen, M. H.; Usseglio, S.; Jakobsen, S.; Olsbye, U.; Tilset, M.; Larabi, C.; Quadrelli, E. A.; Bonino, F.; Lillerud, K. P. Synthesis and Stability of Tagged UiO-66 Zr-MOFs. *Chem. Mater.* **2010**, *22*, 6632.6640.

53. Chusuei, C. C.; Goodman, D. W. X-Ray Pgotoelectron Spectroscopy. *Encyclopedia of Physical Science and Technology*. In *Encyclopedia of Physical Science and Technology, 3rd edition.* R. A. Meyers, ed. Academic Press, NY, 2002, Vol. 17, pp. 921-938.

54. Scrocco, M. Satellite structure in the X-Ray photoelectron spectra of CuO and Cu2O. *Chemical Physics Letter*. **1979**, *63*, 53.

55. XPS- Copper. Thermo Scientific. http://xpssimplified.com/elements/copper.php, last accessed on 06/02/2015.

56. Hu, Z.; Peng, Y.; Kang, Z.; Qian, Y.; Zhao, D. A Modulated Hydrothermal (MHT) Approach for the Facile Synthesis of UiO-66- Type MOFs. *Inorg. Chem*. **2015**, *54*, 4862-4868.

57. Schoenecker, P. M.; Carson, C. G.; Jasuja, H.; Flemming C. J. J.; Walton, K. S. Effect of Water Adsorption on Retention of Structure and Surface Area of Metal-Organic Frameworks. *Ind. Eng. Chem. Res.* **2012**, *51*, 6513-6519.

58. Hartmann, M.; Fischer, M. Amino-functionalized basic catalysts with MIL-101 structure. *Micro. and Meso. Mater.* **2012**, *164*, 38-43.

59. Serra-Crespo, P.; Ramos-Fernandez, E. V.; Gascon, J.; Kapteijn, F. Synthesis and Characterization of an Amino Functionalized MIL-101(Al): Separation and Catalytic Properties. *Chem. Mater.* **2011**, *23*, 2565-2572.

60. Wu, F.; Qiu, L. –G.; Ke, F.; Jiang, X. Copper nanoparticles embedded in metal-organic framework MIL-101(Cr) as a high performance catalyst for reduction of aromatic nitro compounds. *Inorg. Chem. Commun.* **2013**, *32*, 5-8.

61. Pan, H.; Li, X.; Zhang, D.; Guan, Y.; Wu, P. Pt nanoparticles in mesoporous metal-organic frameworks MIL-101 as an efficient and recyclable catalyst for the asymmetric hydrogenation of α- ketoesters. *J. Mol. Catal. A-Chem.* **2013**, *377*, 108-114.

62. Peterson, G. W.; DeCoste, J. B.; Fatollahi-Fard, F.; Britt, D. K. Engineering UiO-66-NH2 for Toxic Gas Removal. *Ind. Eng. Chem. Res.* **2014**, *53*, 701-707.

63. Schaate, A.; Roy, P.; Godt, A.; Lippke, J.; Waltz, F.; Wiebcke, M.; Behrens, P. Modulated Synthesis of Zr-Based Metal-Organic Frameworks: From Nano to Single Crystals. *Chem. Eur. J.* **2011**, *17*, 6643-6651.

64. Katz, M. J.; Brown, Z. J.; Colón, Y. J.; Siu, P. W.; Scheidt, K. A.; Snurr, R. Q.; Hupp, J. T.; Farha, O. K. A facile synthesis of UiO-66, UiO-67 and their derivatives. *Chem. Commun.* **2013**, *49*, 9449.

65. DeCoste, J. B.; Demasky, T. J.; Katz, M. J.; Farha, O. K.; Hupp, J. T. A UiO-66 analogue with uncoordinated carboxylic acids for the broad spectrum removal of toxic chemicals. *New J. Chem.* **2015**, *39*, 2396-2399.